THE JOURNAL OF IMMUNOLOGY

Ecto-Nucleoside Triphosphate Diphosphohydrolase 7 Controls Th17 Cell Responses through Regulation of Luminal ATP in the Small Intestine

Takashi Kusu, Hisako Kayama, Makoto Kinoshita, Seong Gyu Jeon, Yoshiyasu Ueda, Yoshiyuki Goto, Ryu Okumura, Hiroyuki Saiga, Takashi Kurakawa, Kayo Ikeda, Yuichi Maeda, Jun-ichi Nishimura, Yasunobu Arima, Koji Atarashi, Kenya Honda, Masaaki Murakami, Jun Kunisawa, Hiroshi Kiyono, Meinoshin Okumura, Masahiro Yamamoto and Kiyoshi Takeda

J Immunol 2013; 190:774-783; Prepublished online 14 December 2012;
doi: 10.4049/jimmunol.1103067
http://www.jimmunol.org/content/190/2/774

The Journal of Immunology is published twice each month by The American Association of Immunologists, Inc., 9650 Rockville Pike, Bethesda, MD 20814-3994.

Print ISSN: 0022-1767 Online ISSN: 1550-6606.

Ecto-Nucleoside Triphosphate Diphosphohydrolase 7 Controls Th17 Cell Responses through Regulation of Luminal ATP in the Small Intestine

Takashi Kusu,[*,†] Hisako Kayama,[*,‡,§] Makoto Kinoshita,[*,§] Seong Gyu Jeon,[*,‡] Yoshiyasu Ueda,[*] Yoshiyuki Goto,[¶] Ryu Okumura,[*,‡] Hiroyuki Saiga,[*] Takashi Kurakawa,[*] Kayo Ikeda,[*,‡] Yuichi Maeda,[*,‡] Jun-ichi Nishimura,[*] Yasunobu Arima,[‖] Koji Atarashi,[*] Kenya Honda,[*] Masaaki Murakami,[§,‖] Jun Kunisawa,[¶,#] Hiroshi Kiyono,[§,¶] Meinoshin Okumura,[†] Masahiro Yamamoto,[*,‡,§] and Kiyoshi Takeda[*,‡,§]

Extracellular ATP is released from live cells in controlled conditions, as well as dying cells in inflammatory conditions, and, thereby, regulates T cell responses, including Th17 cell induction. The level of extracellular ATP is closely regulated by ATP hydrolyzing enzymes, such as ecto-nucleoside triphosphate diphosphohydrolases (ENTPDases). ENTPDase1/CD39, which is expressed in immune cells, was shown to regulate immune responses by downregulating the ATP level. In this study, we analyzed the immunomodulatory function of ENTPDase7, which is preferentially expressed in epithelial cells in the small intestine. The targeted deletion of *Entpd7* encoding ENTPDase7 in mice resulted in increased ATP levels in the small intestinal lumen. The number of Th17 cells was selectively increased in the small intestinal lamina propria in *Entpd7*$^{-/-}$ mice. Th17 cells were decreased by oral administration of antibiotics or the ATP antagonist in *Entpd7*$^{-/-}$ mice, indicating that commensal microbiota-dependent ATP release mediates the enhanced Th17 cell development in the small intestinal lamina propria of *Entpd7*$^{-/-}$ mice. In accordance with the increased number of small intestinal Th17 cells, *Entpd7*$^{-/-}$ mice were resistant to oral infection with *Citrobacter rodentium*. *Entpd7*$^{-/-}$ mice suffered from severe experimental autoimmune encephalomyelitis, which was associated with increased numbers of CD4^{+} T cells producing both IL-17 and IFN-γ. Taken together, these findings demonstrate that ENTPDase7 controls the luminal ATP level and, thereby, regulates Th17 cell development in the small intestine. *The Journal of Immunology*, **2013, 190: 774–783.**

Extracellular ATP was shown to modulate cellular functions via purinergic receptors in the nervous, vascular, and immune system (1–3). In the immune system, the purinergic receptors, such as P2X7 and P2Y2, recognize ATP that is released from damaged and dying cells. P2X7-dependent sensing of ATP leads to activation of the NALP3 inflammasome that induces inflammation via production of IL-1β/IL-18 (4, 5). P2Y2 was shown to mediate recruitment of neutrophils and macrophages into inflammatory sites and clearance of apoptotic cells by phagocytes (6–8). Thus, the innate immune system recognizes extracellular ATP as danger signals to regulate inflammatory responses. In addition to ATP that is released from damaged cells, ATP is released from intact cells under normal conditions and modulates various immune-cellular functions, such as maturation of dendritic cells (DCs) and activation of B and T cells (3, 9). Recently, several reports indicated that ATP modulates mucosal immune responses by influencing the function of intestinal epithelial cells (ECs) and T cells (10–13). Extracellular ATP was also shown to directly modulate T cell responses through P2X receptors, leading to the induction of intestinal inflammation (14, 15).

Therefore, the level of extracellular ATP is closely regulated to prevent uncontrolled ATP-mediated cellular responses by surface-expressing enzymes that hydrolyze ATP, such as members of the ecto-nucleoside triphosphate diphosphohydrolase (ENTPDase) family, consisting of eight members (ENTPDase1–8) (16–18). Among them, ENTPDase1 (also known as CD39), which is highly

*Laboratory of Immune Regulation, Department of Microbiology and Immunology, Graduate School of Medicine, Osaka University, Suita, Osaka 565-0871, Japan; [†]Department of General Thoracic Surgery, Graduate School of Medicine, Osaka University, Suita, Osaka 565-0871, Japan; [‡]Laboratory of Mucosal Immunology, World Premier International Immunology Frontier Research Center, Osaka University, Suita, Osaka 565-0871, Japan; [§]Core Research for Evolutional Science and Technology, Japan Science and Technology Agency, Saitama 332-0012, Japan; [¶]Division of Mucosal Immunology, Department of Microbiology and Immunology, Institute of Medical Science, University of Tokyo, Tokyo 108-8639, Japan; [‖]Laboratory of Developmental Immunology, Graduate School of Frontier Biosciences, Graduate School of Medicine and World Premier International Immunology Frontier Research Center, Osaka University, Osaka 565-0871, Japan; and [#]Laboratory of Vaccine Materials, National Institute of Biomedical Innovation, Osaka 567-0085, Japan

Received for publication October 25, 2011. Accepted for publication November 8, 2012.

This work was supported by a Grant-in-Aid from the Ministry of Education, Culture, Sports, Science and Technology; the Ministry of Health, Labour and Welfare; and the Osaka Foundation for the Promotion of Clinical Immunology.

Address correspondence and reprint requests to Prof. Kiyoshi Takeda, Laboratory of Immune Regulation, Department of Microbiology and Immunology, Graduate School of Medicine, Osaka University, Suita, Osaka 565-0871, Japan. E-mail address: ktakeda@ongene.med.osaka-u.ac.jp

The online version of this article contains supplemental material.

Abbreviations used in this article: DC, dendritic cell; EAE, experimental autoimmune encephalomyelitis; EC, epithelial cell; ENTPDase, ecto-nucleoside triphosphate diphosphohydrolase; MLN, mesenteric lymph node; MOG, myelin oligodendrocyte glycoprotein; oATP, oxidized ATP; SFB, segmented filamentous bacteria.

www.jimmunol.org/cgi/doi/10.4049/jimmunol.1103067

expressed in immune cells, such as T cells, B cells, NK cells, DCs, and monocytes/macrophages (19, 20), was shown to possess anti-inflammatory activities through ATP hydrolysis. Indeed, severe inflammation was induced in mice lacking ENTPDase1/CD39 in several inflammatory models, including inflammatory bowel disease (21–24). Combinational activity of ENTPDases such as CD39 with CD73 ecto-5′-nucleotidase, which hydrolyzes AMP to adenosine, was also demonstrated in regulatory T cells and intestinal ECs (11, 20, 25). Thus, the immune-modulatory functions of ENTPDase1/CD39 have been well characterized. However, it remains unclear whether other ENTPDase family members are involved in the regulation of immune responses.

In this study, we analyzed the role of ENTPDase7, which was selectively expressed in ECs in the small intestine. Deletion of ENTPDase7 in mice resulted in increased ATP concentrations in the small intestinal lumen and increased numbers of IL-17–producing Th17 cells in the small intestinal lamina propria. Blockade of ATP action decreased the number of Th17 cells in the small intestine of ENTPDase7-deficient mice. In accordance with the increased Th17 cell number, ENTPDase7-deficient mice showed high resistance to the intestinal pathogen *Citrobacter rodentium*. These findings demonstrate that intestinal ECs participate in the regulation of Th17 cell responses by controlling intestinal ATP levels.

Materials and Methods

Real-time RT-PCR

RNA samples were prepared from various organs, epithelial layer, and lamina propria of C57BL/6J mice (CLEA Japan) using TRIzol reagent (Invitrogen), from single-cell suspensions using an RNeasy Mini Kit (QIAGEN), or from laser-microdissected tissue sections using an RNeasy Micro Kit (QIAGEN). Total RNA was reverse transcribed using Moloney murine leukemia virus reverse transcriptase (Promega) and random primers (Toyobo) after treatment with RQ1 DNase I (Promega). cDNA was analyzed by real-time RT-PCR using GoTaq qPCR Master Mix (Promega) in an ABI 7300 real-time PCR system (Applied Biosystems). Values were then normalized to the expression of *Gapdh*, and the fold difference in expression relative to that of *Gapdh* is shown. The following primer sets were used: *Entpd1*, 5′-TGGTGCAGCAGTTAGAGGAATG-3′ and 5′-CGCACCGATTTCATCTGTTTT-3′; *Entpd7*, 5′-CCCCTTTACATCCTCTGCAC-3′ and 5′-GTCAAACTCCAACGGCAAAT-3′; *Muc2*, 5′-ACATCACCTGTCCCGACTTC-3′ and 5′-GAGCAAGGGACTCTGGTCTG-3′; *Krt7*, 5′-ACGGCTGCTGAGAATGAGTT-3′ and 5′-CGTGAAGGGTCTTGAGGAAG-3′; and *Gapdh*, 5′-CCTCGTCCCGTAGACAAAATG-3′ and 5′-TCTCCACTTTGCCACTGCAA-3′.

Isolation of epithelium and lamina propria

Intestines were opened longitudinally, washed to remove fecal content, and incubated in PBS containing 30 mM EDTA for 5 min. Epithelial layer was peeled off from intestines and used as epithelium. For isolation of lamina propria, after removing the epithelial layer, fat tissue was also removed from intestines.

Laser microdissection

The frozen sections (10 μm) of the small intestine were fixed with acetic acid/ethyl alcohol (1:19) for 3 min, followed by H&E staining. Tissues containing >100 goblet cells, absorptive enterocytes, and lamina propria cells were collected by a laser microdissection device (DM6000B; Leica, Tokyo, Japan).

Generation of Entpd7-deficient mice

The targeting vector was constructed by replacement of a 1.0-kb fragment encoding the fourth and fifth exons of *Entpd7* with a neomycin resistance gene cassette, and a gene encoding HSV thymidine kinase driven by a phosphoglycerate kinase promoter was inserted into the genomic fragment for negative selection. After the targeting vector was transfected into V6.5 embryonic stem cells, G418 and ganciclovir double-resistant colonies were selected and screened by PCR and Southern blot analysis. Homologous recombinants were microinjected into blastocysts of C57BL/6 female mice, and heterozygous F1 progeny mice were intercrossed to obtain *Entpd7*-deficient mice. *Entpd7*-deficient mice and their wild-type littermates from these intercrosses were confirmed by Southern blot analysis and Northern blot analysis and were used for experiments. *Entpd7*-deficient mice were backcrossed onto C57BL/6 mice for at least four generations, and *Entpd7*-deficient mice and their wild-type littermates from intercrosses of heterozygous mice were used for experiments. All animal experiments were conducted in accordance with the guidelines of the Animal Care and Use Committee of Osaka University.

Isolation of lymphocytes

To prepare single-cell suspensions from spleens, mesenteric lymph nodes (MLNs), and Peyer's patches, the collected organs were ground between glass slides, and the cells were passed through 40-μm nylon meshes and suspended in PBS. Splenocytes were treated with RBC lysis buffer (0.15 M NH_4Cl, 1 mM $KHCO_3$, 0.1 mM EDTA) for 5 min before suspension. Naive $CD4^+$ T cells were purified using a FACSAria system as $CD4^+CD25^-CD44^{low}CD62L^{high}$ cells. For isolation of intraepithelial lymphocytes, intestines were opened longitudinally, washed to remove fecal content, and shaken in HBSS containing 5 mM EDTA for 20 min at 37°C. After filtration through nylon mesh, the EC fraction was washed with RPMI 1640 containing 4% FBS, resuspended in 5 ml 40% Percoll (GE Healthcare), and overlaid on 2.5 ml 80% Percoll in a 15-ml Falcon tube. Percoll-gradient separation was performed by centrifugation at 780 × *g* for 20 min at 25°C. The intraepithelial lymphocytes were collected at the interface of the Percoll gradient and washed with RPMI 1640 containing 10% FBS. For isolation of lamina propria lymphocytes, intestines were opened, washed to remove fecal content, shaken in HBSS containing 5 mM EDTA for 20 min at 37°C to remove ECs and fat tissue, cut into small pieces, and incubated with RPMI 1640 containing 4% FBS, 1 mg/ml collagenase D (Roche), 0.5 mg/ml dispase (Invitrogen), and 40 μg/ml DNase I (Roche) for 1 h at 37°C in a shaking water bath. The digested tissues were washed with HBSS containing 5 mM EDTA and subjected to Percoll density–gradient centrifugation as for isolation of intraepithelial lymphocytes. The lamina propria lymphocytes were collected at the interface of the Percoll gradient and washed with RPMI 1640 containing 10% FBS.

Intracellular cytokine staining

Intracellular expression of IL-17, IFN-γ, and IL-10 in $CD4^+$ T cells was analyzed using a Cytofix/Cytoperm Kit Plus (with GolgiStop; BD Biosciences), according to the manufacturer's instructions. In brief, lymphocytes obtained from the intestinal lamina propria, spleens, MLNs, or Peyer's patches were incubated with 50 ng/ml PMA (Sigma), 5 μM calcium ionophore A23187 (Sigma), and GolgiStop at 37°C for 4 h. Surface staining was performed with anti–CD4-PerCP/Cy5.5 (BioLegend) for 20 min at 4°C, the cells were permeabilized with Cytofix/Cytoperm solution for 20 min at 4°C, and intracellular cytokine staining was performed with anti–IL-17A–Alexa Fluor 647 (BD Biosciences), anti–IL-10–PE (BD Biosciences), and anti–IFN-γ–FITC (BioLegend) for 20 min. For intracellular staining of Foxp3, cells were stained using the Foxp3 Staining Buffer set (eBiosciences).

Flow cytometry

The following Abs were used for flow cytometry: anti–CD4-PerCP/Cy5.5, anti–CD8α–Pacific Blue, anti–CD3-FITC, anti–TCRγδ-PE, anti–TCRβ-FITC, anti–CD8β–Alexa Fluor 647, and anti–CD4-PE/Cy7 (all from BioLegend); anti–B220-PE, anti–CD3-PE/Cy7, and anti–CD8α-PE (all from BD Biosciences); and anti–TCRγδ-FITC (eBioscience). Anti–Foxp3–Alexa Fluor 647 (eBioscience) was also used, according to the manufacturer's instructions. Data were acquired using a FACSCanto II (BD Biosciences) and analyzed using FlowJo software (Tree Star).

Establishment of small intestinal EC lines

H-2Kb-tsA58–transgenic mice (26) were backcrossed to C57BL/6 mice for six generations. To establish the small intestinal EC lines from wild-type and $Entpd7^{-/-}$ mice, the mice were crossed with H-2Kb-tsA58–transgenic mice. Small intestinal ECs were isolated, as previously described (27), before incubation at 33°C. To confirm that they were intestinal ECs, a single-cell suspension was prepared and cytospun onto the glass slides. After fixation, the cells were incubated with polyclonal anti-cytokeratin Ab (1:500; Dako) and then treated with a ChemMate EnVision kit (Dako). DAB (Dako) was used as a chromogen. Images were taken using a BZ-9000 fluorescence microscope (Keyence).

Measurement of ATP

Feces from individual mice were collected, weighed, and gently suspended in PBS containing 0.01% NaN_3. After centrifugation, the supernatants were collected, and the levels of ATP were determined with a luciferin-

luciferase assay using the ATP assay kit (Toyo Ink), according to the manufacturer's instructions. To analyze ATP levels in the small intestinal tissues, the small intestine was isolated and cut into quarters longitudinally. Each piece was weighed and lysed to measure ATP with a luciferin-luciferase assay. To analyze ATP levels in the EC lines, single-cell suspensions of the indicated cell lines were prepared. The cells were counted and lysed to measure ATP with a luciferin-luciferase assay. For determination of luminal ATP levels, the mice were fasted overnight and anesthetized by i.p. injection with 350 μl 0.5% pentobarbital sodium (Dainippon Sumitomo Pharma). The peritoneal cavity was opened, and the small intestine was ligated with nylon threads at 1.5 and 4.5 cm distal from the Treitz ligament (for the proximal region of the small intestine) or at 3 and 6 cm proximal from the ileum end (for the distal region of the small intestine) to make a closed intestinal loop. A total of 300 ml PBS or 1.5 mM ATP solution was applied luminally with a 29-G needle. The luminal fluid was recovered 15 min later using a 29-G needle and suspended in PBS. After centrifugation, the supernatants were collected, and the levels of ATP were determined with a luciferin-luciferase assay.

Measurement of NTP hydrolyzing activity

NTP (ATP, GTP, UTP, and CTP) hydrolyzing activity was measured in crude membranes from wild-type and *Entpd7*$^{-/-}$ small intestinal ECs, as previously described (28). Briefly, ECs were homogenized; after removing nuclei, the crude membrane fraction was separated from the cytosol by centrifugation at 100,000 × *g* for 30 min. To assay NTP hydrolyzing activity, the membrane fraction containing 10 μg total protein was suspended in reaction buffer (20 mM HEPES [pH 7.4], 120 mM NaCl, 5 mM KCl, 0.2 mM EDTA, 1 mM NaN_3, and 0.5 mM Na_3VO_4, with or without 5 mM $CaCl_2$). After incubation for 5 min at 37°C, 5 μl the reaction buffer containing 10 mM NTP was added and incubated for 30 min. NTP hydrolyzing activity was determined by measuring the inorganic phosphate, as described previously (28).

In vitro naive T cell differentiation

Naive T cells were grown for 4 d at 5 × 10^5 cells/ml with plate-bound anti-CD3 (2 mg/ml) in DMEM supplemented with 10% FBS, penicillin, and streptomycin under Th17-polarizing conditions (2 ng/ml TGF-β, 20 ng/ml IL-6, 5 μg/ml anti–IFN-γ, 5 μg/ml anti–IL-4) or Th0 conditions (5 μg/ml anti–IFN-γ, 5 μg/ml anti–IL-4). Then, cells were incubated with 50 ng/ml PMA (Sigma), 5 μM calcium ionophore A23187 (Sigma), and GolgiStop at 37°C for 4 h for flow cytometry analysis.

Treatment with antibiotics

Mice were given a combination of antibiotics containing 500 μg/ml vancomycin (Wako), 1 mg/ml metronidazole, 1 mg/ml ampicillin, and 1 mg/ml neomycin sulfate (all from Nacalai Tesque) in drinking water from birth for 8 wk prior to flow cytometric analysis of the small intestinal lamina propria $CD4^+$ lymphocytes.

Isolation of bacterial DNA

The isolation of bacterial DNA was performed as previously described (29), with some modifications. Briefly, small intestines isolated from littermate mice at 10 wk of age were opened longitudinally, and intestinal contents were collected. Intestinal tissues were washed three times with PBS for 10 s to remove the mucus layer. To collect epithelium-associated bacteria, tissues were further treated by vigorous hand shaking three times for 20 s in PBS containing 0.5% Tween 20 (30). After centrifuging, pellets were suspended in 500 μl TE buffer (10 mM Tris-HCl, 1 mM EDTA [pH 8]). Glass beads and extraction buffer containing TE-saturated phenol and $NaDodSO_4$ solutions were added to the suspension. The mixture was shaken vigorously on a FastPrep FP100 A (BIO 101); this step was repeated after incubation for 10 min at 65°C. After centrifugation, bacterial DNA was precipitated with isopropanol, washed with 70% ethanol, and suspended in 50 μl TE buffer.

Quantitative real-time PCR amplification of 16S rRNA gene sequences

For quantitative analysis of specific bacterial groups in the luminal contents and epithelial layer of the small intestine, quantitative real-time PCR was performed using a LightCycler 480 II (Roche). Bacterial 16S rRNA genes extracted from luminal contents and epithelial surfaces were amplified by bacterial group–specific primers: all bacteria, 5′-ACTCCTACGGGAGGCAGCAGT-3′ and 5′-ATTACCGCGGCTGCTGGC-3′; Lactobacillaceae, 5′-AGCAGTAGGGAATCTTCCA-3′ and 5′-CACCGCTACACATGGAG-3′; segmented filamentous bacteria (SFB), 5′-GACGCTGAGGCATGAGAGCAT-3′ and 5′-GACGGCACGGATTGTTATTCA-3′; *Bacteroides*, 5′-GGTTCTGAGAGGAAGGTCCC-3′ and 5′-GCTGCCTCCCGTAGGAGT-3′; and Clostridiales, 5′-ACTCCTACGGGAGGCAGC-3′ and 5′-GCTTCTTAGTCAGGTACCGTCAT-3′ (31, 32). All reactions were performed in 20 μl using SYBR Green I Master Mix (Roche). Absolute numbers of bacterial 16S rRNA gene copies were determined from standard curves constructed by quantitative PCR of reference plasmids, including 16S rRNA genes isolated from *Lactobacillus johnsonii*, a type strain of *Lactobacillus* obtained from Japan Collection of Microorganisms (JCM No. 2012), murine intestinal *Bacteroides*, *Clostridium*, and SFB.

Treatment with oxidized ATP

Mice were given 100 μl 6 mM oxidized ATP (oATP; ATP periodate oxidized sodium salt; Sigma) i.v. daily for 2 wk prior to flow cytometric analysis of the small intestinal lamina propria $CD4^+$ lymphocytes.

C. rodentium *infection*

C. rodentium (NBRC 105723T) was cultured in Luria–Bertani broth at 37°C for 16 h. Wild-type and *Entpd7*-deficient mice were infected orally with 2 × 10^9 *C. rodentium* in a total volume of 200 μl/mouse. Survival of infected mice was monitored. At 14 d after the infection, spleens were isolated, weighed, and homogenized. Serial dilutions of the homogenates with saline were spread onto MacConkey agar (Merck). After incubation at 37°C for 16 h, the colonies of the appropriate dilutions were counted, and the CFU of bacteria per gram of tissues was calculated. *C. rodentium* colonies were identified as pink colonies.

Experimental autoimmune encephalomyelitis induction in mice

For the induction of experimental autoimmune encephalomyelitis (EAE), mice were immunized s.c. with 100 μg myelin oligodendrocyte glycoprotein $(MOG)_{35-55}$ (Biologica) in 100 μl CFA (Difco) divided among four sites, two on each hind flank. Then, the mice received 250 ng *Bordetella pertussis* toxin (List Biological Laboratories) i.p. on days 0 and 2. The CNS, especially the whole brain and spinal cord, was harvested 17 d after challenge, cut into pieces, and incubated in DMEM containing 2.5 mg/ml collagenase D (Roche) and 1 mg/ml DNase I (Roche) for 20 min at 37°C in a shaking water bath. The digested tissues were resuspended in 5 ml 37% Percoll (GE Healthcare) and then overlaid on 2.5 ml 70% Percoll in a 15-ml tube. Percoll-gradient separation was performed by centrifugation at 500 × *g* for 20 min at room temperature. Lymphocytes were collected at the Percoll gradient interface and washed with RPMI 1640 containing 10% FBS. Mice were assigned scores of 1 to 5 as follows: 0, no clinical signs of EAE; 1, paralyzed tail; 2, loss of coordinated movement; 3, both hind limbs paralyzed; 4, forelimbs paralyzed; and 5, moribund.

Statistical analysis

Differences between control and experimental groups were evaluated by the Student *t* test.

Results

Selective expression of Entpd7 in small intestinal epithelia

ENTPDase1/CD39 encoded by *Entpd1* was shown to modulate inflammatory responses in addition to thrombopoiesis (24, 33, 34). Because the ENTPDase family consists of eight members, we analyzed tissue expression of *Entpd* gene family members. *Entpd1* was preferentially expressed in lymphoid organs, such as the spleen and lymph nodes (Fig. 1A). Of the other *Entpd* genes, we focused on those that showed selective tissue-expression patterns. *Entpd7* was highly expressed in the small intestine (Fig. 1B). The highest *Entpd7* expression was observed in the proximal region of the small intestine, and its expression gradually decreased as the small intestines descended (Fig. 1C). We then analyzed expression of *Entpd7* in the epithelial layers and lamina propria of the small intestine (Fig. 1D). *Entpd7* was predominantly expressed in the ECs of the small intestine. We further analyzed which types of intestinal ECs (i.e., goblet cells or absorptive enterocytes) highly expressed *Entpd7*. Goblet cell–enriched, absorptive enterocyte-enriched, and lamina propria cell–enriched regions were isolated by laser microdissection, and expression of *Entpd7* was analyzed (Fig. 1E). *Entpd7* was highly expressed in absorptive enterocytes, as well as goblet cells characterized by high expression of *Muc2*.

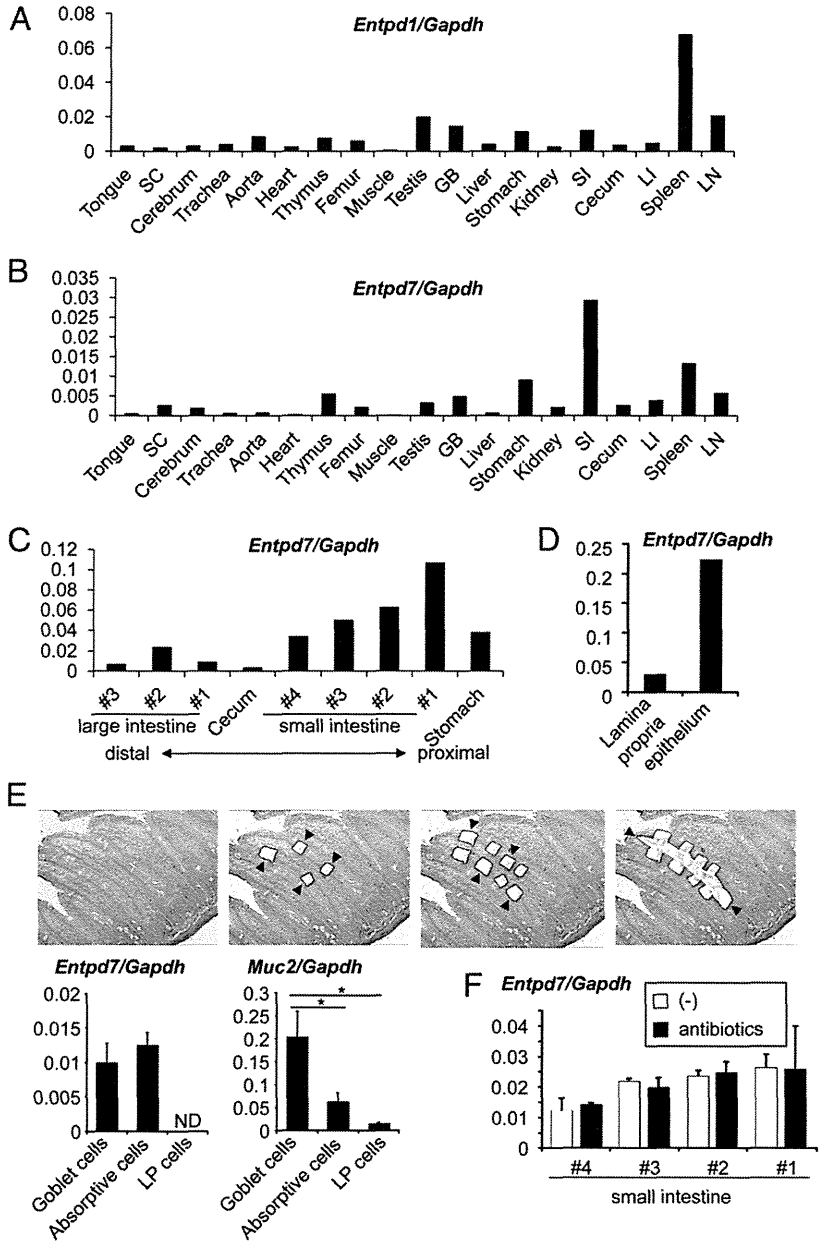

FIGURE 1. High *Entpd7* expression in epithelium of the small intestine. Real-time quantitative RT-PCR analysis of mRNA expression of *Entpd1* (**A**) and *Entpd7* (**B**) in various organs. RNA samples were prepared from various organs of C57BL/6J mice and analyzed by real-time RT-PCR. The values were normalized to that of *Gapdh*. (**C**) Real-time quantitative RT-PCR analysis of *Entpd7* expression in the alimentary tract. The small intestine was cut transversely into four equal pieces, and the colon was cut into three equal pieces. The smaller number denotes the more proximal site of the intestine. Data are representative of three independent experiments. (**D**) Real-time quantitative RT-PCR analysis of *Entpd7* expression in the epithelium and lamia propria of the small intestine. The values were normalized to that of *Gapdh*. Data are representative of three independent experiments. Real-time quantitative RT-PCR analysis of *Entpd7* expression in goblet cells, absorptive ECs, and lamina propria (LP) cells (**E**) and the epithelium of the small intestine (**F**) in mice treated with oral antibiotics. Goblet cell–, absorptive cell–, and lamina propria cell–enriched regions were isolated by laser microdissection. Each region is indicated by arrowheads. H&E staining. Original magnification ×50. The expression of *Muc2*, encoding mucin-2, was also analyzed. The values were normalized to that of *Gapdh*. Data are representative of two independent experiments and represent mean + SD of three mice. $*p < 0.05$. GB, Gall bladder; LI, large intestine; LN, mesenteric lymph node; SC, spinal cord; SI, small intestine.

Thus, *Entpd7* is highly expressed in all types of ECs of the small intestine. Expression of *Entpd7* in the small intestine was not altered in mice treated with oral antibiotics, indicating that *Enptd7* expression is not influenced by microbiota (Fig. 1F).

To assess the physiological function of ENTPDase7 encoded by *Entpd7*, we generated $Entpd7^{-/-}$ mice by gene targeting (Supplemental Fig. 1A, 1B). $Entpd7^{-/-}$ mice were born at the normal Mendelian ratios and grew healthily until 16 wk of age (Supplemental Fig. 1C). Normal lymphocyte development was observed in $Entpd7^{-/-}$ mice (Supplemental Fig. 1D). The composition of lymphocytes in the small and large intestine was not altered in $Entpd7^{-/-}$ mice (Supplemental Fig. 2).

Elevated ATP level in the small intestinal lumen of $Entpd7^{-/-}$ mice

Because ENTPDase is an enzyme that hydrolyzes nucleoside triphosphates, and *Entpd7* was selectively expressed in the small intestinal epithelia, we analyzed concentrations of ATP in the intestine. First, the small intestines were cut into four regions, and their lysates were analyzed for ATP concentration (Fig. 2A). The ATP level was not dramatically altered in any region of the small intestinal tissues between wild-type and $Entpd7^{-/-}$ mice. Because *Entpd7* is highly expressed in ECs of the small intestine, we established intestinal EC lines from wild-type and $Entpd7^{-/-}$ mice using transgenic mice harboring a temperature-sensitive mutation of the SV40 large tumor Ag gene under the control of an IFN-γ–inducible H-$2K^b$ promoter element to analyze ATP levels in the ECs (26, 35, 36). ECs from wild-type and $Entpd7^{-/-}$ mice expressed keratin proteins equally as well as *Krt7* mRNA, indicating that these cells are ECs (Supplemental Fig. 3). *Entpd7* was highly expressed in wild-type ECs but not in $Entpd7^{-/-}$ ECs (Supplemental Fig. 3). Intracellular ATP levels were not altered between wild-type and $Entpd7^{-/-}$ ECs (Fig. 2B). Fecal concentrations of ATP were not different in $Entpd7^{-/-}$ mice compared with wild-type mice (Fig. 2C). However, ATP levels in the luminal contents of the small intestine were substantially increased in $Entpd7^{-/-}$ mice (Fig. 2D). We then created a ligated intestinal loop model to analyze alterations in luminal ATP levels. The proximal regions of the small intestine were ligated to make a loop in wild-type and $Entpd7^{-/-}$ mice. Then, ATP or PBS was injected into the

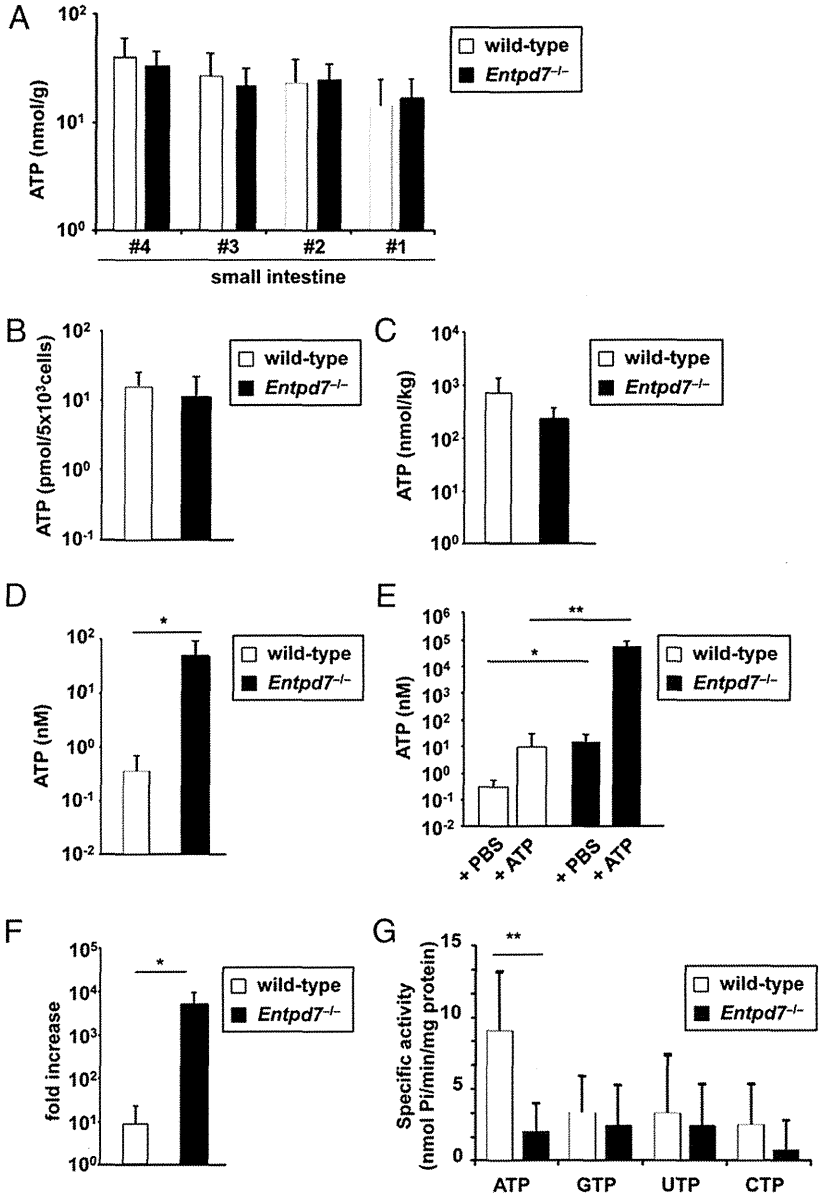

FIGURE 2. Increased luminal ATP levels in the small intestine of *Entpd7*$^{-/-}$ mice. (**A**) The small intestines of wild-type and *Entpd7*$^{-/-}$ mice were cut into quarters transversely. Each piece was weighed and lysed to measure ATP using a luciferin-luciferase assay. The smaller number denotes the more proximal site of the intestine. Data are representative of two independent experiments; means + SD. (**B**) Small intestinal ECs from wild-type and *Entpd7*$^{-/-}$ mice were lysed and analyzed for ATP levels, as described in (A). Data are representative of three independent experiments; means + SD. (**C**) Feces of wild-type and *Entpd7*$^{-/-}$ mice were dissolved in PBS, and ATP levels of the supernatants were measured as described in (A). Data are representative of three independent experiments and represent mean + SD of five mice. (**D**) Wild-type and *Entpd7*$^{-/-}$ mice were anesthetized, peritoneal cavities were opened, and the small intestine was ligated at 1.5 and 4.5 cm distal from the Treitz ligament to make a closed intestinal loop. PBS (300 μl) was injected into the lumen of the small intestinal loop, and the luminal fluid was recovered soon after the injection. ATP levels in the fluid were measured. Data are representative of three independent experiments and represent mean + SD of four mice. (**E**) ATP solution (1.5 mM) or PBS was injected into the intestinal loop, and the luminal fluid was collected 15 min later. ATP levels in the fluids were measured. (**F**) The fold increase in luminal ATP levels after ATP injection in the small intestine of wild-type and *Entpd7*$^{-/-}$ mice. Data are representative of three independent experiments and represent mean + SD of four mice. (**G**) NTP hydrolyzing activity in membrane preparations of intestinal EC lines. Activity for each of the four nucleoside triphosphates was assayed with crude membrane preparations from small intestinal ECs from wild-type and *Entpd7*$^{-/-}$ mice. Data are representative of three independent experiments; means + SD. $*p < 0.05$, $**p < 0.01$.

loop, and ATP levels were analyzed in the luminal contents 15 min later. ATP injection increased luminal ATP levels in wild-type and *Entpd7*$^{-/-}$ mice (Fig. 2E). There was a 10-fold increase observed in ATP-treated wild-type mice. In contrast, the ATP level was increased by >1000-fold in the luminal contents of *Entpd7*$^{-/-}$ mice (Fig. 2F). Thus, *Entpd7*$^{-/-}$ mice show an increased level of luminal ATP, possibly resulting from a serious defect in ATP-clearance activity in the small intestinal lumen. We then measured NTP (ATP, GTP, UTP, and CTP) hydrolyzing activity in membrane preparations of ECs (Fig. 2G). ATP was hydrolyzed most efficiently by the EC membrane fraction of wild-type mice. In addition, the ATP-hydrolyzing activity was severely impaired in the EC membrane fraction of *Entpd7*$^{-/-}$ mice. Thus, small intestinal ECs, which highly express ENTPDase7, have the ability to hydrolyze ATP. These findings indicate that ENTPDase7 is required for the maintenance of ATP levels in the small intestinal lumen.

Increased number of Th17 cells in the small intestinal lamina propria in Entpd7$^{-/-}$ *mice*

A previous study showed that luminal ATP in the intestine mediates Th17 cell development (10). In addition, extracellular ATP was shown to induce Th17 cell development via the inhibition of regulatory T cell functions (15). Therefore, we analyzed the number of CD4$^+$ T cells expressing IL-17, IFN-γ, IL-10, and Foxp3 in the lamina propria of the small and large intestines. The numbers of IL-17–, IFN-γ–, IL-10–, and Foxp3-expressing CD4$^+$ T cells were not altered in the large intestinal lamina propria of *Entpd7*$^{-/-}$ mice (Fig. 3A, 3C). In contrast, the number of IL-17–producing CD4$^+$ T cells in the small intestinal lamina propria was markedly increased in *Entpd7*$^{-/-}$ mice compared with wild-type mice, although the numbers of IFN-γ$^+$, IL-10$^+$, and Foxp3$^+$ T cells were not affected (Fig. 3B, 3C). The number of IL-17–producing CD4$^+$ T cells was not increased in other lymphoid organs, such as the spleen, MLNs, and Peyer's patches of *Entpd7*$^{-/-}$ mice (Supplemental Fig. 4). Thus, *Entpd7*$^{-/-}$ mice showed elevation of Th17 cells in the small intestinal lamina propria. Consistent with *Entpd7*-expression patterns in the small intestine, the level of luminal ATP was higher in the distal region than in the proximal region of the small intestine of wild-type mice (Fig. 3D); accordingly, the number of IL-17–producing CD4$^+$ T cells was higher in the distal region (Fig. 3E).

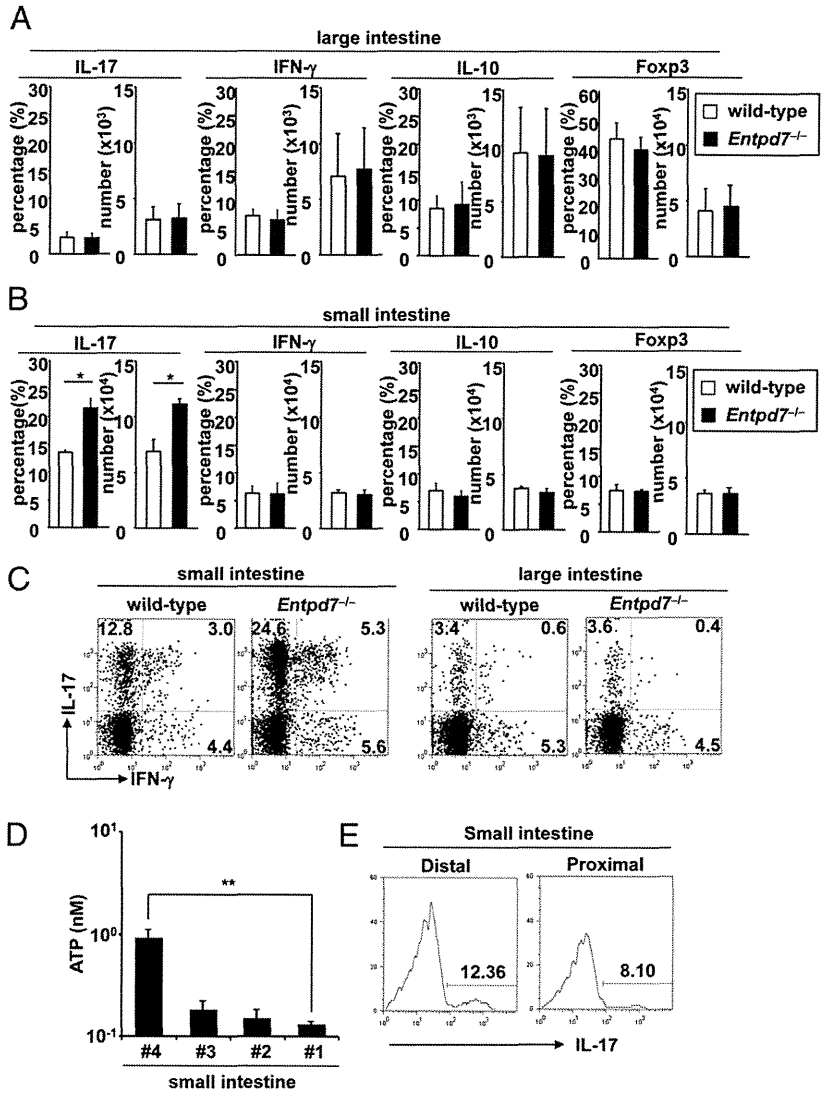

FIGURE 3. Enhanced Th17 cell development in the small intestine of *Entpd7*$^{-/-}$ mice. (**A** and **B**) The lamina propria lymphocytes were isolated from wild-type and *Entpd7*$^{-/-}$ mice, stimulated, permeabilized, stained for IL-17/IFN-γ/IL-10, and analyzed by flow cytometry. Percentages and total numbers of IL-17–, IFN-γ–, and IL-10–producing, as well as Foxp$^+$ CD4$^+$, cells in the large intestinal (A) and the small intestinal (B) lamina propria. Data are mean + SD of four mice. (**C**) Representative FACS dot plots gated on intestinal lamina propria CD4$^+$ cells of wild-type and *Entpd7*$^{-/-}$ mice. (**D**) The level of luminal ATP in the small intestine. The smaller number denotes the more proximal site of the intestine. ATP levels in the luminal fluid in the indicated portions of the small intestine were measured. Data are representative of three independent experiments and represent mean + SD of four mice. (**E**) The numbers of IL-17–producing CD4$^+$ cells in the small intestine. The small intestinal lamina propria lymphocytes were isolated from proximal and distal portions of small intestine of wild-type mice and analyzed for production of IL-17 from CD4$^+$ T cells by flow cytometry. Representative FACS dot plots gated on small intestinal lamina propria CD4$^+$ cells. $*p < 0.05$, $**p < 0.01$.

Commensal microbiota-dependent, ATP-dependent increase in Th17 cells in Entpd7$^{-/-}$ *mice*

We analyzed whether increased Th17 cell development in the small intestine was intrinsic to the T cell itself or caused by extrinsic environmental factors. We first induced in vitro differentiation of splenic naive CD4$^+$ T cells into Th17 cells. Naive CD4$^+$ T cells were cultured in Th17 cell–skewing conditions and analyzed for IL-17 production (Fig. 4A). In vitro–differentiated CD4$^+$ T cells from wild-type and *Entpd7*$^{-/-}$ mice produced almost equal amounts of IL-17, indicating that *Entpd7*$^{-/-}$ T cells were not intrinsically programmed to preferentially differentiate into Th17 cells. We then treated *Entpd7*$^{-/-}$ mice orally with combinations of four antibiotics (i.e., vancomycin, streptomycin, metronidazole, and ampicillin) from birth (Fig. 4B). In antibiotic-treated wild-type and *Entpd7*$^{-/-}$ mice, the number of IL-17–producing T cells, as well as IFN-γ– and IL-10–producing T cells, in the small intestinal lamina propria was dramatically reduced. These findings indicate that the augmentation of Th17 cells in *Entpd7*$^{-/-}$ mice was caused by altered environmental factors influenced by commensal microbiota. Recent data demonstrate that a specific microbiota, such as SFB, induces Th17 cell differentiation in the small intestine (37, 38). Therefore, we analyzed the number of intestinal bacteria in the luminal contents and epithelial layers of the small intestine of wild-type and *Entpd7*$^{-/-}$ mice (Fig. 4C). The number of intestinal bacteria was not altered in *Entpd7*$^{-/-}$ mice, indicating that *Entpd7* deficiency did not cause alteration of microbiota.

Because commensal microbiota were shown to influence luminal ATP level (10), we analyzed the effect of the blockade of ATP action. oATP, which antagonizes P2X receptors, was shown to be effective in modulating T cell responses in mice, especially Th17 cell responses (15). Therefore, *Entpd7*$^{-/-}$ mice were treated with oATP; however, the total number of CD4$^+$ cells in the small intestinal lamina propria was not altered (Fig. 5A). In accordance with the previous finding that oATP inhibits T cell responses, such as cytokine production (14), the number of IFN-γ$^+$ and IL-10$^+$ CD4$^+$ T cells was moderately reduced (Fig. 5B). Notably, the number of IL-17–producing CD4$^+$ T cells was severely reduced in oATP-treated *Entpd7*$^{-/-}$ mice (Fig. 5C, 5D). In an intestinal inflammation model of immunocompromised *Cd3e*$^{-/-}$ mice transferred with conventional T cells, oATP treatment increased the number of Foxp3$^+$ CD4$^+$ T cells in MLNs of the diseased mice (14). However, *Entpd7*$^{-/-}$ mice treated with oATP did not show any increase in the number of Foxp3$^+$ T cells in MLNs or the small intestinal lamina propria (Fig. 5E). Thus, the ATP antagonist severely decreased Th17 cells and moderately reduced IFN-γ– and IL-10–producing T cells. These findings indicate that the increased ATP level is responsible for enhanced Th17 cell development in the small intestine of *Entpd7*$^{-/-}$ mice.

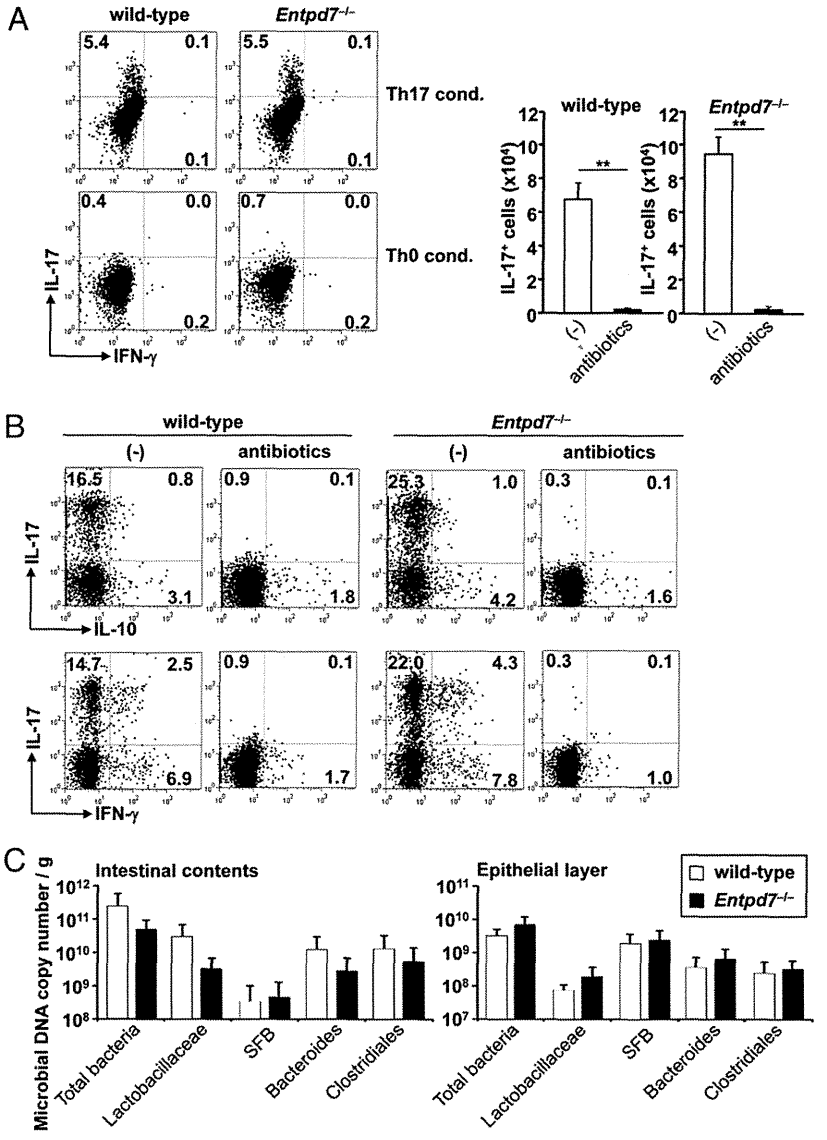

FIGURE 4. Decreased number of Th17 cells in antibiotic-treated *Entpd7*$^{-/-}$ mice. (**A**) Splenic naive CD4$^+$ T lymphocytes were cultured for 4 d under Th17-polarizing conditions (TGF-β, IL-6, anti–IFN-γ, and anti–IL-4) or Th0 conditions (anti–IFN-γ and anti–IL-4). Then, lymphocytes were harvested, stimulated, permeabilized, stained for IL-17 and IFN-γ, and analyzed by flow cytometry. Data are representative of three independent experiments. (**B**) Wild-type (n = 4) and *Entpd7*$^{-/-}$ (n = 4) mice were administered vancomycin, metronidazole, ampicillin, and neomycin sulfate in drinking water from birth. The small intestinal lamina propria lymphocytes were isolated at 8 wk of age and analyzed for production of IL-17, IFN-γ, and IL-10 from CD4$^+$ T cells by flow cytometry. Representative FACS dot plots and total numbers of cells gated on small intestinal lamina propria CD4$^+$ cells are shown. (**C**) Intestinal bacteria in the luminal contents and epithelial layers of the small intestines of wild-type and *Entpd7*$^{-/-}$ mice. DNA isolated from the luminal contents and epithelial layers of the small intestines was analyzed by real-time quantitative PCR using primers for bacterial group–specific 16S rRNA genes. Data are representative of two independent experiments and are mean + SD of five mice.

Resistance to intestinal C. rodentium *infection in Entpd7*$^{-/-}$ *mice*

A previous study showed that development of Th17 cells in the small intestine provides the resistance to oral infection with *C. rodentium* (38). Therefore, we orally infected wild-type and *Entpd7*$^{-/-}$ mice with *C. rodentium*. The CFU titers of bacteria in the spleen were measured at day 14 after the infection (Fig. 6A, 6B). The number of spleens that was invaded with *C. rodentium* was dramatically decreased in *Entpd7*$^{-/-}$ mice. Accordingly, *Entpd7*$^{-/-}$ mice had decreased numbers of *C. rodentium* in the spleen compared with wild-type mice. In addition, although some wild-type mice died after the oral *C. rodentium* infection, none of the *Entpd7*$^{-/-}$ mice died (Fig. 6C). Thus, *Entpd7*$^{-/-}$ mice are resistant to the intestinal bacterium *C. rodentium*.

Deteriorated EAE in Entpd7$^{-/-}$ *mice*

Enhanced Th17 responses are implicated in the development of several immune disorders, including EAE (39). Th17 cells, which develop in the small intestine, were also shown to induce inflammation in extraintestinal tissues, such as arthritis in the ankle joints (40). Furthermore, commensal microbiota were shown to be involved in the pathogenesis of EAE (41). Therefore, we used a MOG peptide–induced model of EAE in *Entpd7*$^{-/-}$ mice to determine the effect of ENTPDase7-mediated regulation of intestinal Th17 cells in inflammatory conditions in vivo. As shown in Fig. 7A, s.c. immunization of wild-type mice with the MOG peptide, together with pertussis toxin, induced encephalomyelitis associated with rapidly ascending paralysis appearing at approximately day 10–12. MOG peptide–immunized *Entpd7*$^{-/-}$ mice showed more severe clinical symptoms. We then analyzed cytokine production from CD4$^+$ T cells infiltrated into the CNS of the diseased mice (Fig. 7B). In wild-type and *Entpd7*$^{-/-}$ mice, infiltration of IL-17– and IFN-γ–producing CD4$^+$ T cells, as well as IL-17/IFN-γ double-producing cells, was observed. IL-17/IFN-γ double-producing CD4$^+$ cells increased markedly in *Entpd7*$^{-/-}$ mice compared with diseased wild-type mice. Thus, in the absence of *Entpd7*, severe EAE developed that was accompanied by an increased infiltration of CD4$^+$ T cells producing both IL-17 and IFN-γ.

Discussion

In the current study, we analyzed the physiological function of ENTPDase7, which is preferentially expressed in ECs of the small intestine. ENTPDase7 deficiency in mice led to increased ATP levels in the small intestinal lumen, indicating that ENTPDase7 is responsible for the maintenance of luminal ATP levels. The number of IL-17–producing Th17 cells in the small intestinal lamina propria was increased in *Entpd7*$^{-/-}$ mice. The number of Th17

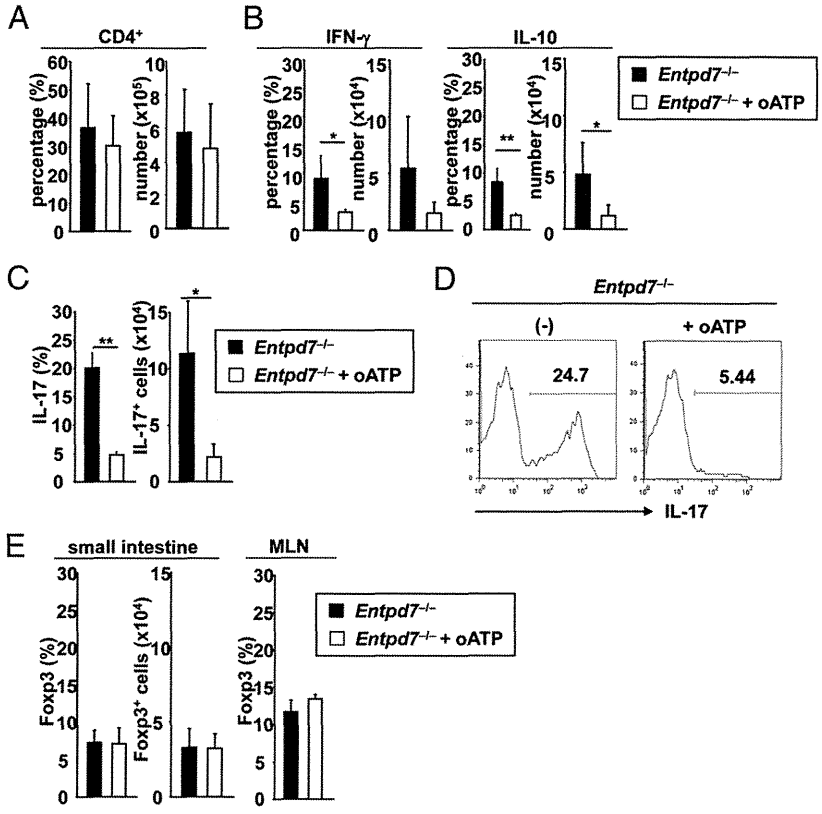

FIGURE 5. Decreased number of Th17 cells in oATP-treated *Entpd7*$^{-/-}$ mice. (**A–C**) *Entpd7*$^{-/-}$ mice were administered 100 μl of 6 mM oATP or PBS i.v. daily for 2 wk. The small intestinal lamina propria lymphocytes were then isolated and analyzed for production of IFN-γ, IL-10, and IL-17 from CD4$^+$ T cells by flow cytometry. The percentages and total numbers of CD4$^+$ T cells (A), IFN-γ and IL-10–producing CD4$^+$ T cells (B), and IL-17–producing CD4$^+$ T cells (C) in the small intestinal lamina propria of PBS- or oATP-treated *Entpd7*$^{-/-}$ mice. Data are representative of two independent experiments and are mean + SD of four mice. (**D**) Representative FACS graph showing IL-17 production gated on small intestinal lamina propria CD4$^+$ T cells of the indicated mice. (**E**) The percentages and total numbers of Foxp3$^+$ CD4$^+$ T cells in the small intestinal lamina propria and MLNs of PBS- or oATP-treated *Entpd7*$^{-/-}$ mice. Data are representative of two independent experiments and are mean + SD of three mice. $*p < 0.05$, $**p < 0.01$.

cells was decreased in *Entpd7*$^{-/-}$ mice in the absence of commensal microbiota or after ATP antagonist treatment. *Entpd7*$^{-/-}$ mice were resistant to infection with *C. rodentium*, against which Th17-related cytokines play a major role.

A previous report indicated that human ENTPDase7 is expressed in the membrane of intracellular compartments (28). The intracellular ATP level, which was analyzed using total-cell lysates, was not altered in *Entpd7*$^{-/-}$ ECs. However, given that the ATP concentration in the cytoplasm is >1 mM, whereas the ATP concentration in the extracellular compartment is usually <10 nM, ATP levels within the ENTPDase7-expressing cellular vesicles of ECs would be increased in the absence of ENTPDase7. Indeed, the membrane fraction of intestinal ECs had an enzymatic activity to hydrolyze ATP, and its activity was decreased in the absence of *Entpd7*. Because Entpd7 was highly expressed in goblet cells, as well as absorptive ECs, it is possible that *Entpd7* is

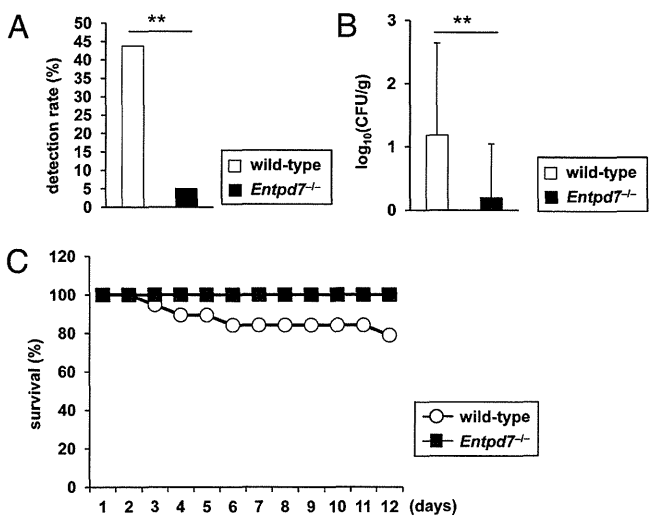

FIGURE 6. Resistance to intestinal *C. rodentium* infection in *Entpd7*$^{-/-}$ mice. (**A–C**) Wild-type (n = 19) and *Entpd7*$^{-/-}$ (n = 19) mice were infected orally with *C. rodentium*. (A) Detection rate of *C. rodentium* in the spleen on day 14. The pooled data of two independent experiments are shown. (B) Log_{10} CFU of *C. rodentium* in spleens. (C) Survival rate of the mice at the indicated time points. The pooled data of two independent experiments are shown. $**p < 0.01$.

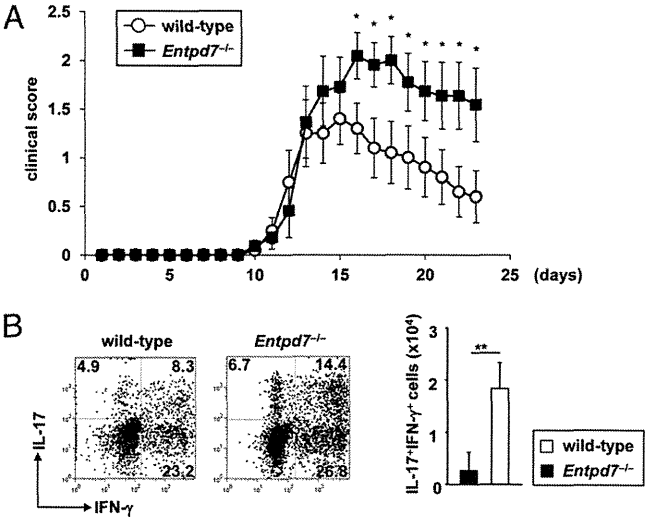

FIGURE 7. Severe EAE in *Entpd7*$^{-/-}$ mice. (**A**) Wild-type (n = 10) and *Entpd7*$^{-/-}$ (n = 11) mice were immunized with 100 μg MOG_{35-55} peptide in CFA; 100 ng of pertussis toxin was injected i.p. on days 0 and 2. The mean clinical score was calculated by averaging the scores of the mice in each group. Data are mean ± SEM at each time point. Experiments were performed twice with similar results. $*p < 0.05$. (**B**) Representative FACS dot plots gated on CD4$^+$ cells of the CNS in the indicated mice at day 17 after EAE induction (*left* and *middle panels*). CNS lymphocytes were isolated from wild-type and *Entpd7*$^{-/-}$ mice 17 d after EAE induction and analyzed for the production of IFN-γ and IL-17 from CD4$^+$ T cells by flow cytometry (*right panel*). Data are representative of five mice analyzed. $**p < 0.05$.

expressed in the membrane of mucin-containing vacuoles of goblet cells to control ATP levels in the vacuole. Given that goblet cells of the airway were shown to secrete ATP, as well as mucin (42), intestinal goblet cells might be a major source of luminal ATP, the level of which is closely regulated by ENTPDase7.

Human ENTPDase7 was shown to preferentially hydrolyze UTP, GTP, and CTP rather than ATP (28). However, the membrane fraction of mouse intestinal ECs effectively hydrolyzed ATP, and its activity was impaired by *Entpd7* deficiency. Thus, mouse ENTPDase7, unlike human ENTPDase7, effectively hydrolyzes ATP. Indeed, apparent differences in amino acid sequences are observed in a domain between the second and third apyrase-conserved regions, supporting that mouse and human ENTPDase7 have different substrate affinities.

Luminal ATP is supposed to be derived from ECs, as discussed above. In addition, commensal microbiota are a source of luminal ATP (10). In this regard, commensal microbiota, especially SFB, mediate Th17 cell development in the small intestine, possibly through ATP-independent mechanisms (37, 43). Therefore, in the small intestine, luminal ATP may mediate Th17 cell development cooperatively with Th17-inducing commensal microbiota. There is controversy as to how luminal ATP is sensed and induces Th17 development. Intestinal CX_3CR1^+ DCs were shown to extrude their dendrites into the lumen to sample intestinal Ags (44, 45). These intestinal DCs might sense luminal ATP via purinergic receptors. Alternatively, as reported in several studies, ECs sense extracellular ATP (11, 25, 46). Therefore, intestinal ECs trigger inflammatory responses to activate T cell development via ATP sensing. Indeed, intestinal ECs were shown to control DC functions (47).

C. rodentium is an enteric bacterium that colonizes the intestine of mice postinfection. Clearance of *C. rodentium* is shown to be dependent on Th17-related cytokines, such as IL-17 and IL-22 (48, 49). Data showing that mice lacking IL-23, a critical cytokine for Th17 cell development, are highly susceptible to *C. rodentium* infection also indicate that Th17-related cytokines are critical for the resistance to intestinal *C. rodentium* infection (50). Consistent with these facts, $Entpd7^{-/-}$ mice showing an increased number of Th17 cells in the small intestine are highly resistant to intestinal infection with *C. rodentium*. IL-22 and IL-17, which induce production of antibacterial peptides (REGIIIγ and β-defensins) from intestinal ECs (48, 51), are produced from other cell populations, such as innate lymphoid cells and γδT cells (52, 53). Therefore, Th17 cells, together with an innate type of IL-17–producing cells, contribute to intestinal pathogens.

In an EAE model, $CD4^+$ T cells producing both IL-17 and IFN-γ are observed in the CNS (54–56). It is still controversial whether these IL-17/IFN-γ double-producing T cells are Th1 or Th17 cells, but they do contribute to EAE pathogenesis (54). A study using $Il23ra^{-/-}$ mice, which showed a reduced number of Th17 cells, as well as IL-17/IFN-γ double-producing T cells and a normal number of Th1 cells, suggested that IL-17/IFN-γ double-producing T cells are derived from Th17 cells (57). Therefore, increased numbers of IL-17/IFN-γ double-producing T cells in the CNS of $Entpd7^{-/-}$ mice with EAE might be due to enhanced Th17 responses.

It remains unclear how Th17 cells residing in the small intestine mediate EAE. However, several lines of evidence indicate the relevance between gut immune cells and immune disorders in extraintestinal tissues: Th17 cells induced by SFB in the small intestinal lamina propria were shown to be responsible for the induction of autoimmune arthritis (40); alteration of the commensal flora composition influences the severity of EAE (41); and SFB-induced Th17 cells in the small intestine induce EAE (58). Thus, intestinal effector T cells are responsible for the induction of immune disorders in nongut tissues, including the CNS, and our present study demonstrates that enhanced intestinal Th17 responses can induce severe inflammatory conditions in these disease models.

In this study, we showed that an ENTPDase expressed by intestinal ECs regulates luminal ATP levels and, thereby, controls intestinal immune responses. Another ENTPDase, ENTPDase8, is selectively expressed by the ECs in the large intestine, as well as the small intestine (T. Kusu and K. Takeda, unpublished observations). Characterization of ENTPDase8 functions in terms of regulation of intestinal immune responses will be an interesting issue to be addressed in the future.

Acknowledgments

We thank C. Hidaka for secretarial assistance and Y. Magota for technical assistance.

Disclosures

The authors have no financial conflicts of interest.

References

1. Burnstock, G. 2007. Physiology and pathophysiology of purinergic neurotransmission. *Physiol. Rev.* 87: 659–797.
2. Vassort, G. 2001. Adenosine 5′-triphosphate: a P2-purinergic agonist in the myocardium. *Physiol. Rev.* 81: 767–806.
3. Junger, W. G. 2011. Immune cell regulation by autocrine purinergic signalling. *Nat. Rev. Immunol.* 11: 201–212.
4. Piccini, A., S. Carta, S. Tassi, D. Lasiglié, G. Fossati, and A. Rubartelli. 2008. ATP is released by monocytes stimulated with pathogen-sensing receptor ligands and induces IL-1beta and IL-18 secretion in an autocrine way. *Proc. Natl. Acad. Sci. USA* 105: 8067–8072.
5. Yu, H. B., and B. B. Finlay. 2008. The caspase-1 inflammasome: a pilot of innate immune responses. *Cell Host Microbe* 4: 198–208.
6. Chen, Y., R. Corriden, Y. Inoue, L. Yip, N. Hashiguchi, A. Zinkernagel, V. Nizet, P. A. Insel, and W. G. Junger. 2006. ATP release guides neutrophil chemotaxis via P2Y2 and A3 receptors. *Science* 314: 1792–1795.
7. Elliott, M. R., F. B. Chekeni, P. C. Trampont, E. R. Lazarowski, A. Kadl, S. F. Walk, D. Park, R. I. Woodson, M. Ostankovich, P. Sharma, et al. 2009. Nucleotides released by apoptotic cells act as a find-me signal to promote phagocytic clearance. *Nature* 461: 282–286.
8. Kronlage, M., J. Song, L. Sorokin, K. Isfort, T. Schwerdtle, J. Leipziger, B. Robaye, P. B. Conley, H. C. Kim, S. Sargin, et al. 2010. Autocrine purinergic receptor signaling is essential for macrophage chemotaxis. *Sci. Signal.* 3: ra55.
9. Trautmann, A. 2009. Extracellular ATP in the immune system: more than just a "danger signal". *Sci. Signal.* 2: pe6.
10. Atarashi, K., J. Nishimura, T. Shima, Y. Umesaki, M. Yamamoto, M. Onoue, H. Yagita, N. Ishii, R. Evans, K. Honda, and K. Takeda. 2008. ATP drives lamina propria T(H)17 cell differentiation. *Nature* 455: 808–812.
11. Weissmüller, T., E. L. Campbell, P. Rosenberger, M. Scully, P. L. Beck, G. T. Furuta, and S. P. Colgan. 2008. PMNs facilitate translocation of platelets across human and mouse epithelium and together alter fluid homeostasis via epithelial cell-expressed ecto-NTPDases. *J. Clin. Invest.* 118: 3682–3692.
12. Ivison, S. M., M. E. Himmel, M. Mayer, Y. Yao, A. Kifayet, M. K. Levings, and T. S. Steiner. 2011. The stress signal extracellular ATP modulates antiflagellin immune responses in intestinal epithelial cells. *Inflamm. Bowel Dis.* 17: 319–333.
13. Heiss, K., N. Jänner, B. Mähnss, V. Schumacher, F. Koch-Nolte, F. Haag, and H. W. Mittrücker. 2008. High sensitivity of intestinal CD8+ T cells to nucleotides indicates P2X7 as a regulator for intestinal T cell responses. *J. Immunol.* 181: 3861–3869.
14. Schenk, U., A. M. Westendorf, E. Radaelli, A. Casati, M. Ferro, M. Fumagalli, C. Verderio, J. Buer, E. Scanziani, and F. Grassi. 2008. Purinergic control of T cell activation by ATP released through pannexin-1 hemichannels. *Sci. Signal.* 1: ra6.
15. Schenk, U., M. Frascoli, M. Proietti, R. Geffers, E. Traggiai, J. Buer, C. Ricordi, A. M. Westendorf, and F. Grassi. 2011. ATP inhibits the generation and function of regulatory T cells through the activation of purinergic P2X receptors. *Sci. Signal.* 4: ra12.
16. Yegutkin, G. G. 2008. Nucleotide- and nucleoside-converting ectoenzymes: Important modulators of purinergic signalling cascade. *Biochim. Biophys. Acta* 1783: 673–694.
17. Schetinger, M. R., V. M. Morsch, C. D. Bonan, and A. T. Wyse. 2007. NTPDase and 5′-nucleotidase activities in physiological and disease conditions: new perspectives for human health. *Biofactors* 31: 77–98.
18. Robson, S. C., J. Sévigny, and H. Zimmermann. 2006. The E-NTPDase family of ectonucleotidases: Structure function relationships and pathophysiological significance. *Purinergic Signal.* 2: 409–430.
19. Maliszewski, C. R., G. J. Delespesse, M. A. Schoenborn, R. J. Armitage, W. C. Fanslow, T. Nakajima, E. Baker, G. R. Sutherland, K. Poindexter, C. Birks,

et al. 1994. The CD39 lymphoid cell activation antigen. Molecular cloning and structural characterization. *J. Immunol.* 153: 3574–3583.
20. Deaglio, S., K. M. Dwyer, W. Gao, D. Friedman, A. Usheva, A. Erat, J. F. Chen, K. Enjyoji, J. Linden, M. Oukka, et al. 2007. Adenosine generation catalyzed by CD39 and CD73 expressed on regulatory T cells mediates immune suppression. *J. Exp. Med.* 204: 1257–1265.
21. Guckelberger, O., X. F. Sun, J. Sévigny, M. Imai, E. Kaczmarek, K. Enjyoji, J. B. Kruskal, and S. C. Robson. 2004. Beneficial effects of CD39/ecto-nucleoside triphosphate diphosphohydrolase-1 in murine intestinal ischemia-reperfusion injury. *Thromb. Haemost.* 91: 576–586.
22. Friedman, D. J., B. M. Künzli, Y. I. A-Rahim, J. Sevigny, P. O. Berberat, K. Enjyoji, E. Csizmadia, H. Friess, and S. C. Robson. 2009. From the Cover: CD39 deletion exacerbates experimental murine colitis and human polymorphisms increase susceptibility to inflammatory bowel disease. *Proc. Natl. Acad. Sci. USA* 106: 16788–16793.
23. Mizumoto, N., T. Kumamoto, S. C. Robson, J. Sévigny, H. Matsue, K. Enjyoji, and A. Takashima. 2002. CD39 is the dominant Langerhans cell-associated ecto-NTPDase: modulatory roles in inflammation and immune responsiveness. *Nat. Med.* 8: 358–365.
24. Enjyoji, K., K. Kotani, C. Thukral, B. Blumel, X. Sun, Y. Wu, M. Imai, D. Friedman, E. Csizmadia, W. Bleibel, et al. 2008. Deletion of cd39/entpd1 results in hepatic insulin resistance. *Diabetes* 57: 2311–2320.
25. Synnestvedt, K., G. T. Furuta, K. M. Comerford, N. Louis, J. Karhausen, H. K. Eltzschig, K. R. Hansen, L. F. Thompson, and S. P. Colgan. 2002. Ecto-5′-nucleotidase (CD73) regulation by hypoxia-inducible factor-1 mediates permeability changes in intestinal epithelia. *J. Clin. Invest.* 110: 993–1002.
26. Jat, P. S., M. D. Noble, P. Ataliotis, Y. Tanaka, N. Yannoutsos, L. Larsen, and D. Kioussis. 1991. Direct derivation of conditionally immortal cell lines from an H-2Kb-tsA58 transgenic mouse. *Proc. Natl. Acad. Sci. USA* 88: 5096–5100.
27. Evans, G. S., N. Flint, A. S. Somers, B. Eyden, and C. S. Potten. 1992. The development of a method for the preparation of rat intestinal epithelial cell primary cultures. *J. Cell Sci.* 101: 219–231.
28. Shi, J. D., T. Kukar, C. Y. Wang, Q. Z. Li, P. E. Cruz, A. Davoodi-Semiromi, P. Yang, Y. Gu, W. Lian, D. H. Wu, and J. X. She. 2001. Molecular cloning and characterization of a novel mammalian endo-apyrase (LALP1). *J. Biol. Chem.* 276: 17474–17478.
29. Matsuki, T., K. Watanabe, J. Fujimoto, Y. Kado, T. Takada, K. Matsumoto, and R. Tanaka. 2004. Quantitative PCR with 16S rRNA-gene-targeted species-specific primers for analysis of human intestinal bifidobacteria. *Appl. Environ. Microbiol.* 70: 167–173.
30. Gong, J., R. J. Forster, H. Yu, J. R. Chambers, P. M. Sabour, R. Wheatcroft, and S. Chen. 2002. Diversity and phylogenetic analysis of bacteria in the mucosa of chicken ceca and comparison with bacteria in the cecal lumen. *FEMS Microbiol. Lett.* 208: 1–7.
31. Bouskra, D., C. Brézillon, M. Bérard, C. Werts, R. Varona, I. G. Boneca, and G. Eberl. 2008. Lymphoid tissue genesis induced by commensals through NOD1 regulates intestinal homeostasis. *Nature* 456: 507–510.
32. Barman, M., D. Unold, K. Shifley, E. Amir, K. Hung, N. Bos, and N. Salzman. 2008. Enteric salmonellosis disrupts the microbial ecology of the murine gastrointestinal tract. *Infect. Immun.* 76: 907–915.
33. Enjyoji, K., J. Sévigny, Y. Lin, P. S. Frenette, P. D. Christie, J. S. Esch, II, M. Imai, J. M. Edelberg, H. Rayburn, M. Lech, et al. 1999. Targeted disruption of cd39/ATP diphosphohydrolase results in disordered hemostasis and thromboregulation. *Nat. Med.* 5: 1010–1017.
34. Robson, S. C., Y. Wu, X. Sun, C. Knosalla, K. Dwyer, and K. Enjyoji. 2005. Ectonucleotidases of CD39 family modulate vascular inflammation and thrombosis in transplantation. *Semin. Thromb. Hemost.* 31: 217–233.
35. Whitehead, R. H., P. E. VanEeden, M. D. Noble, P. Ataliotis, and P. S. Jat. 1993. Establishment of conditionally immortalized epithelial cell lines from both colon and small intestine of adult H-2Kb-tsA58 transgenic mice. *Proc. Natl. Acad. Sci. USA* 90: 587–591.
36. Saiga, H., J. Nishimura, H. Kuwata, M. Okuyama, S. Matsumoto, S. Sato, M. Matsumoto, S. Akira, Y. Yoshikai, K. Honda, et al. 2008. Lipocalin 2-dependent inhibition of mycobacterial growth in alveolar epithelium. *J. Immunol.* 181: 8521–8527.
37. Gaboriau-Routhiau, V., S. Rakotobe, E. Lécuyer, I. Mulder, A. Lan, C. Bridonneau, V. Rochet, A. Pisi, M. De Paepe, G. Brandi, et al. 2009. The key role of segmented filamentous bacteria in the coordinated maturation of gut helper T cell responses. *Immunity* 31: 677–689.
38. Ivanov, I. I., K. Atarashi, N. Manel, E. L. Brodie, T. Shima, U. Karaoz, D. Wei, K. C. Goldfarb, C. A. Santee, S. V. Lynch, et al. 2009. Induction of intestinal Th17 cells by segmented filamentous bacteria. *Cell* 139: 485–498.
39. El-behi, M., A. Rostami, and B. Ciric. 2010. Current views on the roles of Th1 and Th17 cells in experimental autoimmune encephalomyelitis. *J. Neuroimmune Pharmacol.* 5: 189–197.
40. Wu, H. J., I. I. Ivanov, J. Darce, K. Hattori, T. Shima, Y. Umesaki, D. R. Littman, C. Benoist, and D. Mathis. 2010. Gut-residing segmented filamentous bacteria drive autoimmune arthritis via T helper 17 cells. *Immunity* 32: 815–827.
41. Yokote, H., S. Miyake, J. L. Croxford, S. Oki, H. Mizusawa, and T. Yamamura. 2008. NKT cell-dependent amelioration of a mouse model of multiple sclerosis by altering gut flora. *Am. J. Pathol.* 173: 1714–1723.
42. Okada, S. F., L. Zhang, S. M. Kreda, L. H. Abdullah, C. W. Davis, R. J. Pickles, E. R. Lazarowski, and R. C. Boucher. 2011. Coupled nucleotide and mucin hypersecretion from goblet-cell metaplastic human airway epithelium. *Am. J. Respir. Cell Mol. Biol.* 45: 253–260.
43. Ivanov, I. I., and D. R. Littman. 2010. Segmented filamentous bacteria take the stage. *Mucosal Immunol.* 3: 209–212.
44. Rescigno, M., M. Urbano, B. Valzasina, M. Francolini, G. Rotta, R. Bonasio, F. Granucci, J. P. Kraehenbuhl, and P. Ricciardi-Castagnoli. 2001. Dendritic cells express tight junction proteins and penetrate gut epithelial monolayers to sample bacteria. *Nat. Immunol.* 2: 361–367.
45. Niess, J. H., S. Brand, X. Gu, L. Landsman, S. Jung, B. A. McCormick, J. M. Vyas, M. Boes, H. L. Ploegh, J. G. Fox, et al. 2005. CX3CR1-mediated dendritic cell access to the intestinal lumen and bacterial clearance. *Science* 307: 254–258.
46. Schwiebert, E. M., and A. Zsembery. 2003. Extracellular ATP as a signaling molecule for epithelial cells. *Biochim. Biophys. Acta* 1615: 7–32.
47. Rescigno, M., U. Lopatin, and M. Chieppa. 2008. Interactions among dendritic cells, macrophages, and epithelial cells in the gut: implications for immune tolerance. *Curr. Opin. Immunol.* 20: 669–675.
48. Ishigame, H., S. Kakuta, T. Nagai, M. Kadoki, A. Nambu, Y. Komiyama, N. Fujikado, Y. Tanahashi, A. Akitsu, H. Kotaki, et al. 2009. Differential roles of interleukin-17A and -17F in host defense against mucoepithelial bacterial infection and allergic responses. *Immunity* 30: 108–119.
49. Zheng, Y., P. A. Valdez, D. M. Danilenko, Y. Hu, S. M. Sa, Q. Gong, A. R. Abbas, Z. Modrusan, N. Ghilardi, F. J. de Sauvage, and W. Ouyang. 2008. Interleukin-22 mediates early host defense against attaching and effacing bacterial pathogens. *Nat. Med.* 14: 282–289.
50. Mangan, P. R., L. E. Harrington, D. B. O'Quinn, W. S. Helms, D. C. Bullard, C. O. Elson, R. D. Hatton, S. M. Wahl, T. R. Schoeb, and C. T. Weaver. 2006. Transforming growth factor-beta induces development of the T(H)17 lineage. *Nature* 441: 231–234.
51. Wolk, K., S. Kunz, E. Witte, M. Friedrich, K. Asadullah, and R. Sabat. 2004. IL-22 increases the innate immunity of tissues. *Immunity* 21: 241–254.
52. Sutton, C. E., S. J. Lalor, C. M. Sweeney, C. F. Brereton, E. C. Lavelle, and K. H. Mills. 2009. Interleukin-1 and IL-23 induce innate IL-17 production from gammadelta T cells, amplifying Th17 responses and autoimmunity. *Immunity* 31: 331–341.
53. Spits, H., and J. P. Di Santo. 2011. The expanding family of innate lymphoid cells: regulators and effectors of immunity and tissue remodeling. *Nat. Immunol.* 12: 21–27.
54. Abromson-Leeman, S., R. T. Bronson, and M. E. Dorf. 2009. Encephalitogenic T cells that stably express both T-bet and ROR gamma t consistently produce IFNgamma but have a spectrum of IL-17 profiles. *J. Neuroimmunol.* 215: 10–24.
55. Korn, T., M. Mitsdoerffer, A. L. Croxford, A. Awasthi, V. A. Dardalhon, G. Galileos, P. Vollmar, G. L. Stritesky, M. H. Kaplan, A. Waisman, et al. 2008. IL-6 controls Th17 immunity in vivo by inhibiting the conversion of conventional T cells into Foxp3+ regulatory T cells. *Proc. Natl. Acad. Sci. USA* 105: 18460–18465.
56. Suryani, S., and I. Sutton. 2007. An interferon-gamma-producing Th1 subset is the major source of IL-17 in experimental autoimmune encephalitis. *J. Neuroimmunol.* 183: 96–103.
57. McGeachy, M. J., Y. Chen, C. M. Tato, A. Laurence, B. Joyce-Shaikh, W. M. Blumenschein, T. K. McClanahan, J. J. O'Shea, and D. J. Cua. 2009. The interleukin 23 receptor is essential for the terminal differentiation of interleukin 17-producing effector T helper cells in vivo. *Nat. Immunol.* 10: 314–324.
58. Lee, Y. K., J. S. Menezes, Y. Umesaki, and S. K. Mazmanian. 2011. Proinflammatory T-cell responses to gut microbiota promote experimental autoimmune encephalomyelitis. *Proc. Natl. Acad. Sci. USA* 108(Suppl. 1): 4615–4622.

THE JOURNAL OF IMMUNOLOGY

Critical Role of Dendritic Cells in T Cell Retention in the Interfollicular Region of Peyer's Patches

Takashi Obata, Naoko Shibata, Yoshiyuki Goto, Izumi Ishikawa, Shintaro Sato, Jun Kunisawa and Hiroshi Kiyono

J Immunol 2013; 191:942-948; Prepublished online 14 June 2013;
doi: 10.4049/jimmunol.1200636
http://www.jimmunol.org/content/191/2/942

The Journal of Immunology is published twice each month by
The American Association of Immunologists, Inc.,
9650 Rockville Pike, Bethesda, MD 20814-3994.

Print ISSN: 0022-1767 Online ISSN: 1550-6606.

Critical Role of Dendritic Cells in T Cell Retention in the Interfollicular Region of Peyer's Patches

Takashi Obata,*,[1] Naoko Shibata,*,†,‡,[1] Yoshiyuki Goto,*,§ Izumi Ishikawa,* Shintaro Sato,*,§ Jun Kunisawa,*,†,‡,¶ and Hiroshi Kiyono*,†,§,‖

Peyer's patches (PPs) simultaneously initiate active and quiescent immune responses in the gut. The immunological function is achieved by the rigid regulation of cell distribution and trafficking, but how the cell distribution is maintained remains to be elucidated. In this study, we show that binding of stromal cell–derived lymphoid chemokines to conventional dendritic cells (cDCs) is essential for the retention of naive CD4$^+$ T cells in the interfollicular region (IFR) of PPs. Transitory depletion of CD11c^{high} cDCs in mice rapidly impaired the IFR structure in the PPs without affecting B cell follicles or germinal centers, lymphoid chemokine production from stromal cells, or the immigration of naive T cells into the IFRs of PPs. The cDC-orchestrated retention of naive T cells was mediated by heparinase-sensitive molecules that were expressed on cDCs and bound the lymphoid chemokine CCL21 produced from stromal cells. These data collectively reveal that interactions among cDCs, stromal cells, and naive T cells are necessary for the formation of IFRs in the PPs. *The Journal of Immunology*, **2013, 191: 942–948.**

Intestinal tissue is located in a harsh environment where it is exposed to a complex mixture of external Ags (including digested food materials) and gut microbiota. The gut immune system creates appropriate homeostatic conditions by discriminating between harmful and beneficial Ags (1, 2). Peyer's patches (PPs) are a major GALT that initiates both active and quiescent immune responses in the gastrointestinal tract (3). The PPs share common immunological features with other secondary lymph nodes (LNs), such as the presence of follicular B cell and paraffollicular T cell regions, but they also show unique immunological characteristics that are used to initiate Ag-specific immune responses against Ags from the gut lumen (3). For instance, PPs contain efferent but not afferent lymphatics, therefore decreasing the opportunity for Ags to be delivered to the PPs via the systemic route. Instead, PPs are covered by follicle-associated epithelium, where Ag-sampling M cells transport luminal Ags into the PPs (4). The area under the follicle-associated epithelium is known as the subepithelial dome, an area where dendritic cells (DCs) are present in abundance and function to capture and process the luminal Ags initially taken up by M cells (5).

PP organogenesis begins embryonically with an immunological interaction between lymphoid-lineage retinoic acid–related orphan receptor γt$^+$IL-7R$^+$CD3$^-$CD4$^+$CD45$^+$ PP inducer cells and mesenchymal-lineage VCAM-1$^+$ICAM-1$^+$ PP organizer cells (6). Binding of lymphotoxin (LT) $\alpha_1\beta_2$ on PP inducer cells to its receptor (LTβR) on PP organizer cells results in the production of lymphoid chemokines (e.g., CXCL13, CCL19, and CCL21) from PP organizer cells. These chemokines recruit T cells, B cells, and DCs into the PPs, leading to the subsequent organization of the immunological microarchitecture of the T cell–rich interfollicular region (IFR) and B cell–rich follicles (6). This architecture enables the efficient induction of Ag-specific immune responses against luminal Ags. Formation of cell clusters of DCs, T cells, and B cells in the PPs leads to the induction and activation of Ag-specific lymphocytes together with the expression of gut-homing molecules such as $\alpha_4\beta_7$ integrin and CCR9 (7, 8). Furthermore, the cellular network creates an optimal molecular and cellular environment for promoting μ-to-α class switch recombination of B cells in the germinal centers (9).

DCs are generally known as Ag processing and presenting cells, but several lines of evidence have recently demonstrated that they are also involved in the maintenance of lymphoid structure in the induced BALT (iBALT) and peripheral LNs (10–12); however, how DCs are involved in the formation of the lymphoid structure of PPs is still obscure. In this study, we show that conventional DCs (cDCs) can bind CCL21 on their surface and retain naive CD4$^+$ T cells in the IFRs of PPs.

*Division of Mucosal Immunology, The Institute of Medical Science, The University of Tokyo, Tokyo 108-8639, Japan; †Department of Medical Genome Science, Graduate School of Frontier Science, The University of Tokyo, Tokyo 108-8639, Japan; ‡Laboratory of Vaccine Materials, National Institute of Biomedical Innovation, Osaka 567-0085, Japan; §Core Research for Evolutional Science and Technology, Japan Science and Technology Agency, Tokyo 102-0075, Japan; ¶Graduate School of Pharmaceutical Sciences, Osaka University, Osaka 565-0871, Japan; and ‖Graduate School of Medicine, The University of Tokyo, Tokyo 113-0033, Japan

[1]T.O. and N.S. contributed equally to this work and therefore share the authorship.

Received for publication February 22, 2012. Accepted for publication May 13, 2013.

This work was supported by grants from the Ministry of Education, Culture, Sports, Science and Technology of Japan (for Scientific Research on Innovative Areas [to J.K.], for Scientific Research [to H.K.], for Challenging Exploratory Research [to J.K.], and for the Leading-Edge Research Infrastructure Program [to J.K. and H.K.]), as well as the Young Researcher Overseas Visits Program for Vitalizing Brain Circulation initiated by the Japan Society for the Promotion of Science (to J.K., H.K., and Y.G.). This work was also supported by grants from the Japan Society for the Promotion of Science Fellows (to N.S.), grants from the Ministry of Health and Welfare of Japan (to J.K. and H.K.), the Global Center of Excellence Program of the Center of Education and Research for Advanced Genome-Based Medicine (to H.K.), the Program for Promotion of Basic and Applied Research for Innovations in Bio-Oriented Industry (to J.K.), and by the Yakult Bio-Science Foundation (to J.K.).

Address correspondence and reprint requests to Dr. Jun Kunisawa and Dr. Hiroshi Kiyono, Division of Mucosal Immunology, Department of Microbiology and Immunology, The Institute of Medical Science, The University of Tokyo, 4-6-1 Shirokanedai, Minato-ku, Tokyo 108-8639, Japan. E-mail addresses: kunisawa@ims.u-tokyo.ac.jp (J.K.) and kiyono@ims.u-tokyo.ac.jp (H.K.)

The online version of this article contains supplemental material.

Abbreviations used in this article: BM, bone marrow; cDC, conventional dendritic cell; DC, dendritic cell; DT, diphtheria toxin; DTR, diphtheria toxin receptor; HEV, high endothelial venule; iBALT, inducible BALT; IFR, interfollicular region; LN, lymph node; LT, lymphotoxin; MLN, mesenteric lymph node; pDC, plasmacytoid dendritic cell; PNA, peanut agglutinin; PP, Peyer's patch; Tg, transgenic; WT, wild-type.

www.jimmunol.org/cgi/doi/10.4049/jimmunol.1200636

Materials and Methods

Mice and in vivo treatment

BALB/c mice were purchased from Japan Clea (Tokyo, Japan). CD11c-diphtheria toxin receptor (DTR) transgenic (Tg) mice (13) and CD11b-DTR Tg mice (14) were obtained from The Jackson Laboratory (Bar Harbor, ME). Paucity of LN T cells (*plt/plt*) mice on a BALB/c background were provided by Drs. H. Nakano and T. Kakiuchi (Department of Immunology, Toho University School of Medicine, Tokyo, Japan) (15). For the depletion of DCs and CD11b$^+$ cells, mice were i.p. injected with 500 ng DT dissolved in PBS (Sigma-Aldrich, St. Louis, MO). Bone marrow (BM)-chimeric mice were established by i.v. transfer of 1×10^7 BM cells into irradiated recipient mice. The recipient mice were rested for 8 wk before use. For the heparinase treatment, mice received an i.v. injection of heparinase mixture (heparitinase and heparinase, 1 U each; Seikagaku, Tokyo, Japan) 16 h before analysis (16). As a control, 1 U chondroitinase ABC (Seikagaku) was similarly injected. Mice were maintained under specific pathogen-free conditions at The Institute of Medical Science (The University of Tokyo), and all experiments were conducted in accordance with the guidelines of the Animal Care and Use Committees of The University of Tokyo.

Cell preparation

For the preparation of mononuclear cells from PPs, a standard physical and enzymatic dissociation protocol was employed as previously described (17). Briefly, PP segments were dissected and agitated vigorously in RPMI 1640 containing 0.5 mM EDTA and 2% FCS to remove epithelial cells. The segments were then agitated in RPMI 1640 containing 2% FCS and 0.5 mg/ml collagenase type IV (Wako Chemicals, Osaka, Japan). Similarly, cells were isolated from the mesenteric LNs (MLNs) by agitation with collagenase type IV.

Flow cytometry and cell sorting

Flow cytometry and cell sorting were performed with FACSCanto II and FACSAria (BD Biosciences, San Diego, CA), respectively, as previously described (18). Briefly, cells were first preincubated with an anti-CD16/CD32 mAb (2.4G2; BD Biosciences) and then stained with fluorescently labeled Abs specific for B220, CD3, CD4, CD8α, CD11b, CD11c, CD31, CD45, CD45RB, CD62L, CD69, or PD1 (all from BD Biosciences), or for FR4 (BioLegend, San Diego, CA). For the detection of peanut agglutinin (PNA), cells were reacted with biotinylated PNA (Vector Laboratories, Burlingame, CA) and subsequently incubated with fluorescently labeled streptavidin. Via-Probe (BD Biosciences) was used to discriminate between dead and living cells.

For the detection of surface binding of CCL21, cells were incubated for 10 min with 1 μg/ml CCL21 (PeproTech, Princeton, NJ). After two washes, the cells were reacted with a purified Ab specific for CCL21 (R&D Systems, Minneapolis, MN) followed by additional incubation with a fluorescently labeled goat IgG-specific Ab. For the heparinase treatment, cells were incubated with 25 mU/ml heparinase mixture for 1 h at 37°C (16). All data were analyzed by using FlowJo software (Tree Star, Ashland, OR).

Immunohistochemistry

PPs, MLNs, and spleens were fixed in 4% paraformaldehyde for 15 h at 4°C, washed, and treated in 20% sucrose for 12 h at 4°C. The tissues were embedded in OCT compound (Sakura Finetek Japan, Tokyo, Japan). Sections were stained with appropriate Abs and the tyramide signal amplification system (PerkinElmer, Shelton, CT) (17). Briefly, cryostat sections (7 μm) were treated with 1% H_2O_2 and an avidin/biotin blocking kit (Vector Laboratories) to quench endogenous peroxidase and biotin. After being blocked with anti-CD16/CD32 Ab in TNT buffer (0.1 M Tris-HCl [pH 7.5], 0.15 M NaCl, 0.05% Tween 20) for 15 min at room temperature, sections were stained with a PE-labeled anti-B220 mAb, biotinylated anti-CD11c mAb, biotinylated anti-CD4 mAb (BD Biosciences), purified anti–reticular fibroblast mAb (ER-TR7; BMA Biomedicals, Augst, Switzerland), fluorescein-conjugated PNA (Vector Laboratories), or purified anti–LYVE-1 polyclonal Ab (R&D Systems). For the detection of ER-TR7 and LYVE-1, the sections were additionally incubated with biotinylated secondary Abs (Jackson ImmunoResearch, West Grove, PA). After washes with TNT buffer, the sections were incubated with HRP-conjugated streptavidin (Pierce, Rockford, IL) for 30 min at 4°C, and the fluorescent signal was amplified by using the tyramide signal amplification system with an appropriate fluorescent dye. After the specimens were stained with DAPI (Sigma-Aldrich), they were analyzed by using a confocal laser-scanning microscope (TCS SP2; Leica, Wetzlar, Germany).

Macro-confocal analysis

CD4$^+$ T cells or purified CD62L^{high} naive T cells (1×10^7) were isolated from PPs and MLNs, labeled with 5 μM CFSE (Invitrogen), and adoptively transferred into recipient mice. A macroscopic view of PPs was obtained by using a macro-confocal microscope (AZ-C1; Nikon, Tokyo, Japan).

Quantitative RT-PCR

Total RNA was isolated with TRIzol reagent (Invitrogen), and cDNA was synthesized from the RNA by using a SuperScript VILO cDNA synthesis kit (Invitrogen). Quantitative RT-PCR was performed with the LightCycler system (Roche Diagnostics, Basel, Switzerland) as reported previously (18). The primers and hybrid probes used for the RT-PCR were as follows: CCL19-specific oligonucleotide primers (sense, 5′-GCCAAGAACAAA-GGCAACA-3′, antisense, 5′-CACACTCACATCGACTCTCTA-3′), an FITC-labeled probe for CCL19 detection (5′-TGGCCCAGGAAACCA-AGGACCA-3′), and a LightCycler Red 640–labeled hybrid probe (5′-AAGAGAGGACCAGGCCTCCT-3′); CCL21-specific oligonucleotide primers (sense, 5′-ACAGACACAGCCCTCAA-3′, antisense, 5′-CATGAG-GTGGCTGCTTT-3′), an FITC-labeled probe for CCL21 detection (5′-CCAGGAGATCCCCCACGAACTTC-3′), and a LightCycler Red 640–labeled hybrid probe (5′-AGCTGGGTGGTTCACGGT-3′); GAPDH-specific oligonucleotide primers (sense, 5′-TGAACGGGAAGCTCACTGG-3′, antisense, 5′-TCCACCACCCTGTTGCTGTA-3′), an FITC-labeled probe for GAPDH detection (5′-CTGAGGACCAGGTTGTCTCCTGCGA-3′), and a LightCycler Red 640–labeled hybrid probe (5′-TTCAACAGCAACT-CCCACTCTTCCACC-3′) (Nihon Gene Research Laboratories, Sendai, Japan).

Statistical analyses

The results were compared using the Student *t* test. The threshold for statistical significance was set at $p < 0.05$.

Results

Depletion of cDCs disrupts T cell regions in the IFR of PPs

To examine the involvement of DCs in the maintenance of PP microarchitecture, we employed a CD11c-DTR Tg mouse system (13). A previous study demonstrated that a single injection of DT into these Tg mice ablated DCs expressing high levels of CD11c in vivo (13, 19). We initially tested whether DT treatment would induce a similar reduction of DCs in the intestinal tissues. We found that the i.p. injection of high amounts of DT (25 ng/g body weight) into CD11c-DTR Tg mice depleted CD11c^{high} cDCs in the PPs, but not CD11c^{int}B220$^+$ plasmacytoid DCs (pDCs) 24 h after the injection (Fig. 1A, 1B). Immunohistochemical analysis indicated that cDCs were depleted in both the subepithelial dome and IFR of the PPs (Fig. 1C). DT treatment did not affect the DC population in wild-type (WT) mice (Supplemental Fig. 2G).

Depletion of cDCs decreases naive CD4$^+$ T cells in the PPs

The depletion of cDCs in CD11c-DTR Tg mice by DT treatment was associated with a small reduction of the T cell population. Indeed, flow cytometric analysis showed that the number of CD3$^+$ T cells decreased in the PPs of CD11c-DTR Tg mice receiving DT. Although PNA$^+$ germinal center B cells were decreased, presumably due to the lack of Ag presentation by cDCs, B220$^+$ B cells and the germinal center distribution were retained (Supplemental Fig. 1A–C). Among CD3$^+$ T cell populations, CD4$^+$ T cells, the dominant T cell population in the PPs, and especially naive CD4$^+$ cells expressing high levels of CD62L and CD45RB were decreased by the DT treatment (Fig. 2A–C, Supplemental Fig. 1D). In contrast, CD69$^+$ activated T cells, FR4$^+$ regulatory T cells, and PD1$^+$ follicular helper T cells were not affected by the DT treatment (Fig. 2B–E).

Consistent with the fact that naive CD4$^+$ T cells are predominantly located in the IFR of PPs (3), immunohistochemical analysis revealed that the IFR structure was disrupted in cDC-depleted mice (Fig. 2F). To examine the T cell distribution at the tissue

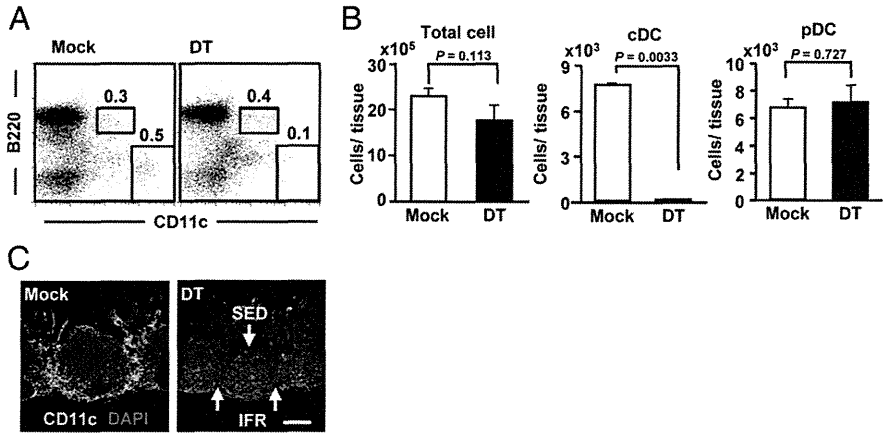

FIGURE 1. Depletion of cDCs in the PPs of CD11c-DTR Tg mice by DT treatment. (**A**) CD11c-DTR Tg mice were given an i.p. injection of DT (*right*) or PBS (mock, *left*). After 24 h, cells were isolated from the PPs for the flow cytometric analysis of CD11c and B220. Data are representative of three independent experiments (three mice per group for each experiment). (**B**) The cell numbers of cDCs (*top*) and pDCs (*bottom*) were calculated from the total cell numbers and cell ratios determined with flow cytometry (n = 3/group; similar results were obtained from three separate experiments). (**C**) Confocal microscopic analysis of the PPs was performed using a CD11c-specific Ab (green) and DAPI (blue) for counterstaining. Data are representative of three independent experiments (three mice per group for each experiment). Scale bar, 300 μm. SED, Subepithelial dome.

level, we employed macro-confocal microscopy (20). When CFSE-labeled $CD62L^{high}$ naive T cells were adoptively transferred into WT mice, T cells accumulated in the IFR of PPs and reached the steady-state 15 h after the transfer. As we previously reported (20), the mesh-like structure of the T cell area was clearly detected in the IFR of PPs (Fig. 2G, mock). Administration of DT to CD11c-DTR Tg mice resulted in the disruption of IFRs throughout the PPs (Fig. 2G, DT). In contrast, T cells were preferentially observed in the follicular area in the PPs of DC-depleted mice (Fig. 2F, 2G). Because cDCs recovered 144 h after the single DT injection, and the disrupted T cell regions and the number of naive T cells were restored with the recovery of cDCs (Fig. 2H, 2I), it seems that the depletion of cDCs was temporary and reversible and the distribution of T cells in the IFR depends on the presence of cDCs.

To exclude the possibility that DT affected nonhematopoietic cells and therefore removed cDCs through an indirect mechanism, we made BM-chimeric mice. Eight weeks after BM transfer from CD11c-DTR Tg mice into irradiated WT mice, the reconstituted WT mice were given DT i.p. These mice also showed depletion of cDCs (Supplemental Fig. 2A) and aberrant T cell organization in the IFR, with a decrease of naive T cells and comparable levels of $FR4^+$ regulatory T cells and $PD1^+$ follicular helper T cells (Supplemental Fig. 2B–D). Additionally, T cells barely expressed CD11c in the PPs (unpublished data), and $B220^+$ cells, including $CD11c^+$ pDCs and $CD11c^-$ B cells, were not affected by the DT treatment (Fig. 1A). To avoid the possibility that excess inflammation induced by cell death might have disrupted the T cell distribution, we analyzed CD11b-DTR Tg mice and confirmed that treatment of CD11b-DTR Tg mice with DT did not affect the distribution of T cells in the PPs (Supplemental Fig. 2E). Together with a previous report that PP structure was maintained in the absence of $RET^+CD3^-CD4^-IL\text{-}7R\alpha^-CD11c^+$ cells, which are key regulatory cells in PP organogenesis and are also susceptible to DT (21, 22), our data collectively indicate that the structure of the IFR with regard to T cells is mediated by cDCs.

We then examined whether the rapid disruption of T cell regions by temporary cDC depletion is specific to PPs or is a more general phenomenon in secondary LNs by investigating MLNs, which drain to PPs, the intestinal lamina propria, and the spleen. The DT treatment barely affected the T cell regions or the number of naive T cells in the MLNs and spleens, despite depletion of the DCs (Supplemental Fig. 3 and unpublished data), as had been previously reported (19, 23). Taken together, these data suggest that the rapid disruption of the T cell regions by the cDC deletion was specific to the IFRs of PPs.

Depletion of cDCs affects T cell retention in, but not immigration into, the PPs

We next examined whether the disruption of IFR T cells by the cDC deletion was due to the inhibition of T cell immigration, retention, or both. We performed macro-confocal imaging in individual mice to observe the distribution of adoptively transferred $CD4^+$ T cells in PPs over time. In this experimental condition, we focused on the surface of PPs to predominantly show images of naive T cells. When $CD4^+$ T cells labeled with CFSE were adoptively transferred into mice, the labeled $CD4^+$ T cells rapidly immigrated into PPs and gradually accumulated in the IFRs; cell motility and accumulation as well as the number of $CFSE^+$ naive T cells and activated T cells in the PPs were similar in the cDC-depleted and mock-treated mice (Fig. 3A). Consistent with the normal immigration of $CD4^+$ T cells into PPs, $LYVE\text{-}1^+$ high endothelial venules (HEVs), a portal site for lymphocyte entry into the PPs, developed normally in the cDC-depleted mice (Fig. 3B).

We then examined the effect of cDC depletion on T cell retention in the IFR of PPs. As mentioned above, T cell accumulation in the IFR of PPs reached the steady-state 15 h after the adoptive transfer. Indeed, a clear T cell region was detected in the IFR of PPs (Fig. 3C). When DT was administered to CD11c-DTR Tg mice 15 h after the adoptive transfer, the IFR structure almost disappeared, and the number of $CFSE^+$ naive T cells in PPs, but not activated T cells, had also decreased 8 h after the DT treatment (Fig. 3C). In contrast, the IFR structure remained normal in the PPs of CD11c-DTR Tg mice without the DT treatment (Fig. 3C). These data indicate that cDCs are specifically involved in T cell retention in the IFR of PPs, but do not affect their immigration into the tissue.

Stromal cells reside normally in the IFR of PPs and produce CCL19 and CCL21 in cDC-depleted mice

Stromal cells in the LNs are thought to play an essential role in the regulation of T cell motility by producing lymphoid chemokines (e.g., CCL19 and CCL21) (15, 24). Consistent with this, we found a disruption of IFR T cells and a decrease of naive $CD4^+$ T cells in

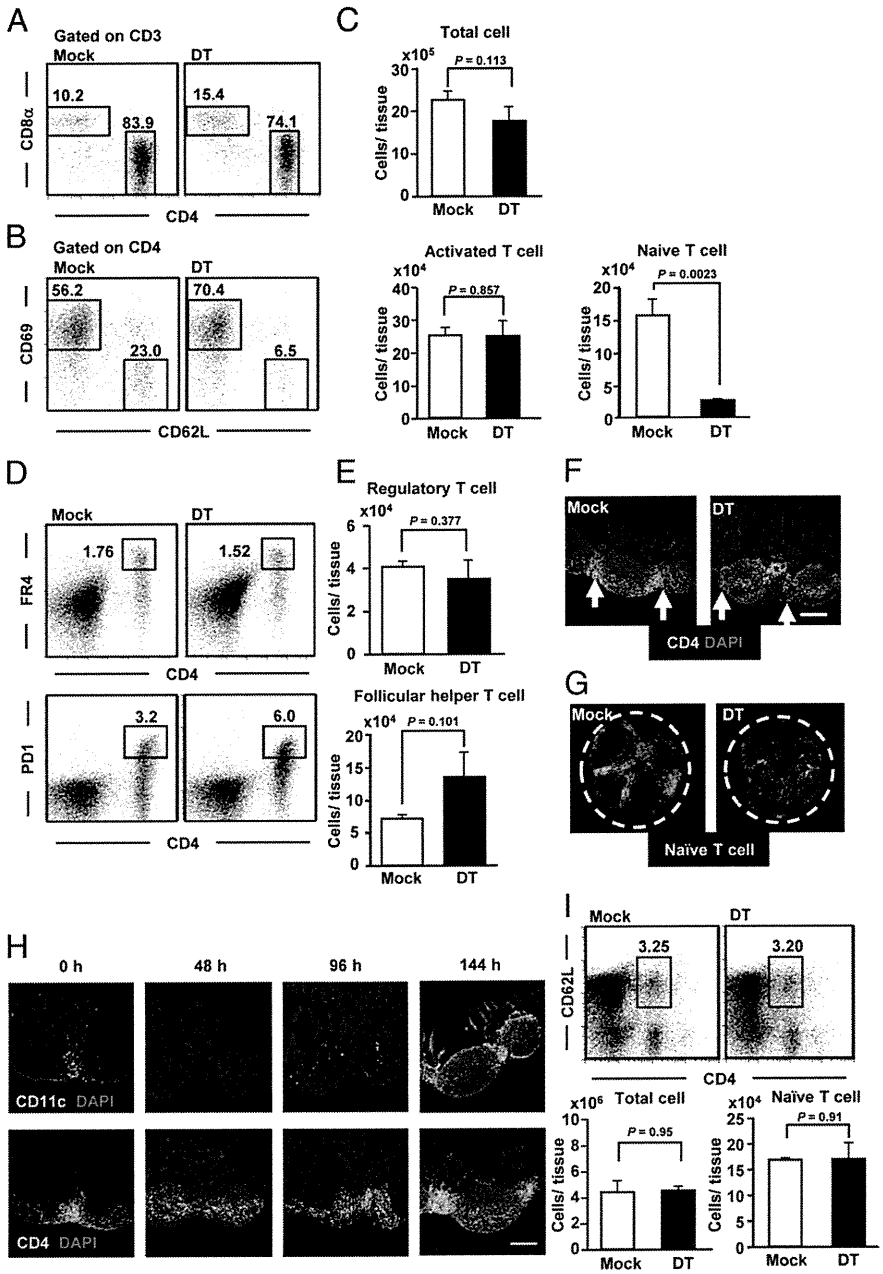

FIGURE 2. Selective reduction of naive $CD4^+$ T cells in the IFRs of PPs by cDC depletion. (**A** and **B**) Flow cytometric analysis was performed 24 h after a DT injection using Abs specific for CD3, CD4, CD8α, CD62L, and CD69. Data are representative of three independent experiments (three mice per group in one experiment). (**C** and **E**) Cells were isolated from one PP and the number of each cells of each type was calculated from the total cell numbers and cell ratios determined with flow cytometry (n = 3/group). Data are representative of three independent experiments. (**D**) Cells were isolated from the PPs for the flow cytometric analysis of CD4 and FR4 (*top*) or PD1 (*bottom*) expression (n = 3/group). Similar results were obtained from three independent experiments. (**F**) Frozen sections of PPs were stained with an Ab specific for CD4 (green) and DAPI (blue). The arrows point to IFRs (n = 3/group). Data are representative of three independent experiments. (**G**) Fifteen hours after the adoptive transfer of CFSE-labeled $CD62L^{high}$ naive T cells into CD11c-DTR Tg mice, the mice were treated with DT. Eight hours after the DT injection, the T cell distribution in the PPs was examined with macro-confocal microscopy. The dotted white lines represent the edges of the PPs. Data are representative of three independent experiments (n = 3/group). (**H**) CD11c-DTR Tg mice received a DT injection. After 0, 48, 96, or 144 h, the animals were sacrificed and frozen sections of PPs were stained with an Ab for CD11c (*top*) or CD4 (*bottom*) together with DAPI (n = 3/group). Data are representative of three independent experiments. (**I**) Flow cytometric analysis was performed 144 h after a DT injection using Abs specific for CD4 and CD62L (*top*). Cells were isolated from one PP and the number of each cells of each type was calculated from the total cell numbers and cell ratios determined with flow cytometry (bottom) (n = 3/group). Data are representative of three independent experiments. Scale bars in (F) and (H), 300 μm.

plt/plt mice, which lack functional CCL19 and CCL21 (Fig. 4A, 4B). Thus, it was possible that cDC depletion affected stromal cells, including their synthesis of chemokines, and thus indirectly induced the disorganized structure of IFR T cell regions in the PPs. To test this possibility, we examined stromal cells in the PPs of CD11c-DTR Tg mice after the DT treatment. Histological and flow cytometric analysis revealed that ER-$TR7^+CD45^-$ stromal cells were present normally at the IFR of PPs of cDC-depleted mice (Fig. 4C, 4D).

We then measured the expression of lymphoid chemokines (CCL19 and CCL21) by stromal cells. We purified $CD45^-$ stromal cells and examined the expression of CCL19 and CCL21 by quantitative RT-PCR. No significant differences were observed between cDC-deleted and intact mice in expression of either CCL19 or CCL21 (Fig. 4E). Taken together, these results suggest that CCL19 and CCL21 are essential for the maintenance of the IFR, but the disorganized IFR in cDC-depleted mice was not due to a disruption in the localization and function of stromal cells.

CCL21 bound to cDCs plays a pivotal role in the maintenance of IFR T cell regions in the PPs

It was previously reported that DCs, as well as stromal cells, produce CCL19 (25). We therefore hypothesized that CCL19 and CCL21 from cDCs play a major role in the localization of T cells in IFR of PPs. To test this hypothesis, we made two types of BM-chimeric mice; in one, irradiated WT mice received adoptive transfer of BM cells from *plt/plt* mice, and in the other, the adoptive transfer was from WT mice to *plt/plt* mice. Normal localization of T cells was noted in the IFRs of PPs in mice lacking the production of CCL19 and CCL21 from hematopoietic cells, including cDCs, whereas disrupted T cell regions were observed in the PPs of BM-chimeric *plt/plt* mice that had received WT BM cells (Fig. 5A). We cannot completely exclude the possibility that endogenous cDCs are retained in BM-chimeric mice. However, if the endogenous cDCs retained $CD4^+$ T cells through the expression of CCL19 and CCL21, we would detect $CD4^+$ T cell retention in both WT mice receiving *plt/plt* BM cells and *plt/plt* mice receiving WT BM cells. In fact,

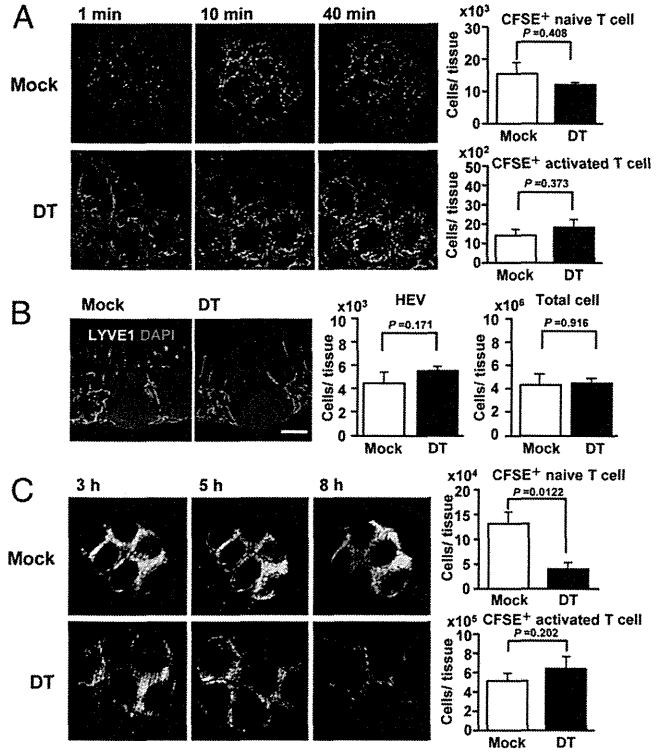

FIGURE 3. Depletion of cDCs affects T cell retention, but not immigration into the PPs. (**A**) CFSE-labeled $CD4^+$ T cells were adoptively transferred into cDC-depleted (DT) or intact (mock) mice. After 1, 10, and 40 min, accumulation of the transferred T cells was examined by macro-confocal microscopy. The number of CFSE-labeled $CD62L^{high}$ naive T cells and $CD69^+$ activated T cells was calculated from the total cell number and cell ratio determined with flow cytometry (n = 3/group). Data are representative of three independent experiments. (**B**) Frozen sections of PPs were prepared from cDC-depleted (DT) and intact (mock) mice for the staining of LYVE-1^+ HEVs and efferent lymphatic vessels (green). Scale bar, 300 μm. The number of $CD31^-CD45^+$ endothelial cells was calculated from the total cell number and cell ratio determined with flow cytometry (n = 3/group). Data are representative of three independent experiments. (**C**) CFSE-labeled $CD4^+$ T cells were adoptively transferred into CD11c-DTR Tg mice. After 15 h, mice received DT or mock (PBS) treatment. Macroscopic distribution of CFSE-labeled T cells in the PPs was examined at the indicated times. CFSE-labeled $CD62L^{high}$ naive T cells and $CD69^+$ activated T cells were counted 8 h after injection of PBS or DT (n = 3/group). Data are representative of three independent experiments.

only WT mice receiving *plt/plt* BM cells had a normal T cell area, whereas *plt/plt* mice receiving WT BM cells showed an impaired T cell area. These findings indicate that, although both cDCs and CCL19/21 are involved in the maintenance of $CD4^+$ T cells in the IFRs of PPs, CCL19 and CCL21 expressed by cDCs are not sufficient to retain $CD4^+$ T cells in the PPs.

Several lines of evidence have demonstrated that chemokines bound to the cell surface can mediate cell motility in vivo (26). Thus, we hypothesized that exogenous CCL19 and CCL21 bound to the surface of cDCs regulate T cell retention. We found that cDCs can bind CCL21 on the cell surface, whereas $CD4^+$ T cells barely bound to CCL21 (Fig. 5B).

Heparan sulfate is a glycosaminoglycan that binds to chemokines in vivo (13). We found that treatment with a heparinase mixture inhibited the binding of CCL21 to the cDCs (Fig. 5C). These findings allowed us to examine the role of heparan sulfate in T cell retention in vivo. As with cDC depletion, treatment of the WT mice with the heparinase mixture led to the disruption of $CD4^+$ T cells and the decrease of naive T cells, whereas chondroitinase ABC, another enzyme that degrades glycosaminoglycans, did not affect the T cell region in the PPs (Fig. 5D). We also confirmed that the heparinase mixture had no additional effect on the IFR structure when cDCs were already depleted (Supplemental Fig. 4).

Discussion

As APCs, DCs strongly adhere to T cells through the immunological synapse, which includes the MHC/TCR complex and costimulatory molecules; this adhesion primes Ag-specific T cell responses (27). In this study, we showed that cDCs also interact with T cells through an immobilized chemokine, CCL21. This chemokine-mediated interaction is required for the retention of T cells, especially naive T cells, in the IFR of PPs, a key organized inductive tissue for the gut immune system. This selective effect on naive T cells can be explained by their high expression of the CCL21 receptor, CCR7. It was previously reported that CCL19 and CCL21 are necessary for the maintenance of IFRs in the PPs and that stromal cells are important in this pathway (15, 24). Our current findings suggest that stromal and T cell interactions are not sufficient, and that DCs are additionally required for the chemokine-mediated maintenance of the IFR structure of PPs. In the cDC-depleted condition, stromal cells were distributed normally in the PPs and expressed levels of CCL19 and CCL21 comparable to those in mice with intact cDCs. Although DCs act as an additional source of CCL19 (25), our experiment using adoptive transfer of BM cells from *plt/plt* mice indicated that the T cell region defects in the IFR were not due to production of chemokines by cDCs. Thus, it is plausible that stromal cell–derived chemokines are captured by cDCs and are then used to retain newly immigrated naive T cells in the IFRs of PPs.

Several lines of evidence have demonstrated the involvement of cDCs in the maintenance of secondary and tertiary LNs (10–12). One study demonstrated that cDCs play a major role in providing an LT signal for the promotion of lymphoid chemokines, especially CXCL13; depletion of cDCs led to the disintegration of the iBALT formed by influenza infection (11). Because CXCL13 recruits mainly B cells (28), these defects were associated with a specific reduction of B cells in the iBALT (11). In contrast to the function of cDCs in iBALT formation, our study demonstrated that cDCs are involved in the retention of T cells in the IFRs without affecting B cell follicles or the germinal center. Another study recently showed that cDCs control lymphocyte entry into LNs by inducing the expression of HEV-associated molecules (e.g., FucT-VII, GlcNAc6ST-2, and the L-selectin counterreceptor GLYCAM1) (12). This study showed that DCs expressing LT directly interacted with HEVs expressing LTβ receptors to induce these molecules. Indeed, impaired lymphocyte migration into the LN in cDC-depleted mice was restored by the adoptive transfer of LT-sufficient, but not LT-deficient, DCs. Of note, the phenotypes were observed in the brachial, inguinal, and cervical LNs, but not PPs (12). Additionally, unlike in our experiments, long-term treatment of CD11c-DTR mice with DT (~8 d) was required to observe these phenotypes. Another study recently reported that semimature DCs reached LNs via the afferent lymph, which is also involved in the T cell homeostasis in the LN (29). They showed that semimature DCs produce vascular endothelial growth factor, which induces the growth and differentiation of HEVs and efficient homing of T cells to LNs. They also showed that semimature DCs not only promote the production of CCL21 from stromal cells but also bind CCL21 via the heparin-binding domain (29). Our study demonstrated that HEVs developed normally in the cDC-depleted mice, and cDCs did not increase the expression of CCL21 from stromal cells, indicating that semimature DCs and

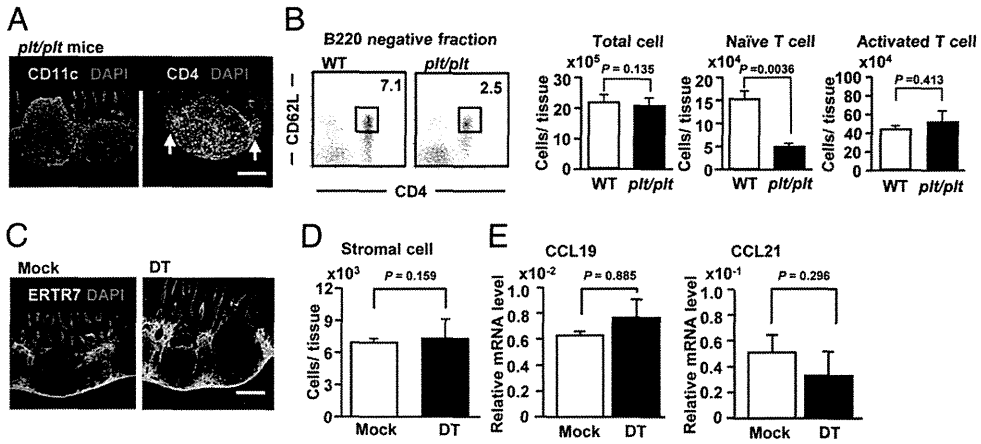

FIGURE 4. Presence of stromal cells expressing CCL19 and CCL21 in the IFRs of cDC-depleted mice. (**A**) Frozen sections of PPs were prepared from *plt/plt* mice for the staining of CD4 (*right*) and CD11c (*left*) (both shown in green). The arrows point to IFRs (n = 3/group). Data are representative of three independent experiments. (**B**) Cells were isolated from the PPs for the flow cytometric analysis of CD4 and CD62L expression, and the number of $CD62L^{high}$ naive T cells and $CD69^+$ activated T cells was calculated (n = 3/group). Data are representative of three independent experiments. (**C**) Frozen sections of PPs were prepared from cDC-depleted (DT) and intact (mock) mice for the staining of $ER\text{-}TR7^+$ stromal cells (green) (n = 3/group). Data are representative of three independent experiments. Scale bar, 300 μm. (**D**) Cells were isolated from one PP and the number of $CD45^-$ stromal cells was calculated from the total cell number and cell ratio determined with flow cytometry (n = 3/group). Data are representative of three independent experiments. (**E**) Quantitative RT-PCR analysis of CCL19 and CCL21 expression on stromal cells from the PPs of cDC-depleted (DT) and intact (mock) mice. The data are presented as the ratio to GAPDH mRNA (mean ± SD, n = 4). Data are representative of three independent experiments.

cDCs regulate T cell distribution in different ways. These findings suggest that PP cDCs have a unique function in regulating T cell retention.

The selective phenotype of PP T cells in cDC-depleted mice could be explained by the sensitive ability of PP DCs to bind CCL21 through the expression of heparin or heparinase-sensitive

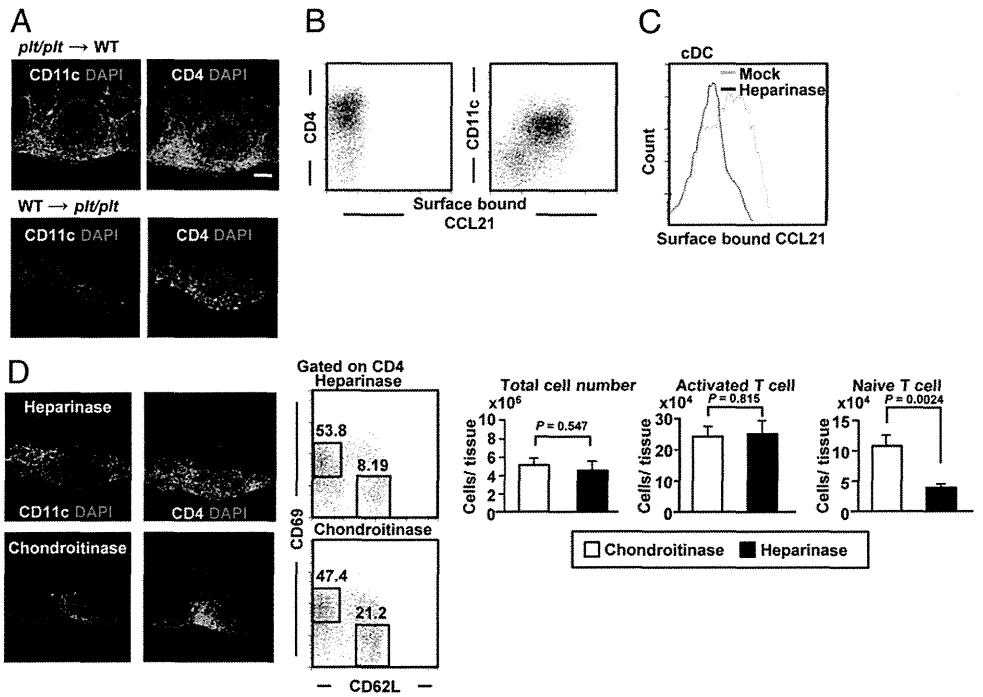

FIGURE 5. cDCs are not the main producers of CCL19 and CCL21, but bind exogenous CCL19 and CCL21. (**A**) PP tissue sections were prepared from irradiated WT mice receiving BM cells from *plt/plt* mice (*top*) or vice versa (*bottom*). PP sections were stained with Abs for CD11c (*left*) and CD4 (*right*) (n = 3/group). Data are representative of three independent experiments. Scale bar, 300 μm. (**B**) Sorted $CD4^+$ T cells (*left*) and cDCs (*right*) from PPs were preincubated for 10 min with 1 μg/ml CCL21 and then incubated with a purified goat Ab specific for CCL21. The cells were then stained with fluorescently labeled Abs specific for goat IgG, CD4, and CD11c and subjected to flow cytometry (n = 3 per group). Data are representative of three independent experiments. (**C**) Sorted heparinase- (black) or mock-treated (blue) cDCs from PPs were preincubated for 10 min with 1 μg/ml CCL21 and then incubated with a purified goat Ab specific for CCL21. The cells were then stained with fluorescently labeled Abs specific for goat IgG and subjected to flow cytometry (n = 3/group). Data are representative of three independent experiments. (**D**) WT mice received an i.v. injection of heparinase mixture (heparitinase and heparinase, 1 U each) or 1 U chondroitinase ABC. After 16 h, PP tissue sections were prepared for the staining of CD11c (*left*) and CD4 (*right*). Cells were isolated from the PPs for the flow cytometric analysis of CD4 and CD62L expression (*upper right*). Cells were isolated from one PP and the number of $CD62L^{high}$ naive T cells and $CD69^+$ activated T cells was calculated from the total cell number and cell ratio determined with flow cytometry (n = 3/group). Data are representative of three independent experiments.

molecules. Subset-specific expression of heparan sulfate was reported in mast cells (30). Indeed, highly differentiated connective tissue–type mast cells, but not mucosal mast cells, express high levels of heparin (30). Heparin biosynthesis is mediated by multiple complex steps involving many enzymes such as *N*-deacetylase/*N*-sulfotransferase and exostoses-1 (31, 32). Exostoses-1 is required for the formation of heparan sulfate chains that bind to CCL21 on endothelial cells (16). The involvement of these pathways is the subject of our next study.

In summary, we have shown that PP cDCs sensitively bind to CCL21 at low concentration through the heparan sulfate chain, and this interaction is necessary for maintaining the IFR structure of PPs by retaining naive $CD4^+$ T cells. These findings provide new evidence for the unique immunological functions of gut DCs in the maintenance of immunological microarchitecture, in particular the IFR of the PP, a key organized lymphoid structure in the gut immune system.

Acknowledgments

We thank Dr. T. Okada (RIKEN Research Center for Allergy and Immunology, Yokohama, Japan) for helpful discussions.

Disclosures

The authors have no financial conflicts of interest.

References

1. Hill, D. A., and D. Artis. 2010. Intestinal bacteria and the regulation of immune cell homeostasis. *Annu. Rev. Immunol.* 28: 623–667.
2. Kiyono, H., J. Kunisawa, J. R. McGhee, and J. Mestecky. 2008. The mucosal immune system. In *Fundamental Immunology.* W. E. Paul, ed. Lippincott-Raven, Philadelphia, p. 983–1030.
3. Kunisawa, J., T. Nochi, and H. Kiyono. 2008. Immunological commonalities and distinctions between airway and digestive immunity. *Trends Immunol.* 29: 505–513.
4. Kraehenbuhl, J. P., and M. R. Neutra. 2000. Epithelial M cells: differentiation and function. *Annu. Rev. Cell Dev. Biol.* 16: 301–332.
5. Johansson, C., and B. L. Kelsall. 2005. Phenotype and function of intestinal dendritic cells. *Semin. Immunol.* 17: 284–294.
6. Eberl, G., and M. Lochner. 2009. The development of intestinal lymphoid tissues at the interface of self and microbiota. *Mucosal Immunol.* 2: 478–485.
7. Iwata, M., A. Hirakiyama, Y. Eshima, H. Kagechika, C. Kato, and S. Y. Song. 2004. Retinoic acid imprints gut-homing specificity on T cells. *Immunity* 21: 527–538.
8. Mora, J. R., M. Iwata, B. Eksteen, S. Y. Song, T. Junt, B. Senman, K. L. Otipoby, A. Yokota, H. Takeuchi, P. Ricciardi-Castagnoli, et al. 2006. Generation of gut-homing IgA-secreting B cells by intestinal dendritic cells. *Science* 314: 1157–1160.
9. Fagarasan, S., S. Kawamoto, O. Kanagawa, and K. Suzuki. 2010. Adaptive immune regulation in the gut: T cell-dependent and T cell-independent IgA synthesis. *Annu. Rev. Immunol.* 28: 243–273.
10. Halle, S., H. C. Dujardin, N. Bakocevic, H. Fleige, H. Danzer, S. Willenzon, Y. Suezer, G. Hämmerling, N. Garbi, G. Sutter, et al. 2009. Induced bronchus-associated lymphoid tissue serves as a general priming site for T cells and is maintained by dendritic cells. *J. Exp. Med.* 206: 2593–2601.
11. GeurtsvanKessel, C. H., M. A. Willart, I. M. Bergen, L. S. van Rijt, F. Muskens, D. Elewaut, A. D. Osterhaus, R. Hendriks, G. F. Rimmelzwaan, and B. N. Lambrecht. 2009. Dendritic cells are crucial for maintenance of tertiary lymphoid structures in the lung of influenza virus-infected mice. *J. Exp. Med.* 206: 2339–2349.
12. Moussion, C., and J. P. Girard. 2011. Dendritic cells control lymphocyte entry to lymph nodes through high endothelial venules. *Nature* 479: 542–546.
13. Jung, S., D. Unutmaz, P. Wong, G. Sano, K. De los Santos, T. Sparwasser, S. Wu, S. Vuthoori, K. Ko, F. Zavala, et al. 2002. In vivo depletion of $CD11c^+$ dendritic cells abrogates priming of $CD8^+$ T cells by exogenous cell-associated antigens. *Immunity* 17: 211–220.
14. Stoneman, V., D. Braganza, N. Figg, J. Mercer, R. Lang, M. Goddard, and M. Bennett. 2007. Monocyte/macrophage suppression in CD11b diphtheria toxin receptor transgenic mice differentially affects atherogenesis and established plaques. *Circ. Res.* 100: 884–893.
15. Nakano, H., S. Mori, H. Yonekawa, H. Nariuchi, A. Matsuzawa, and T. Kakiuchi. 1998. A novel mutant gene involved in T-lymphocyte-specific homing into peripheral lymphoid organs on mouse chromosome 4. *Blood* 91: 2886–2895.
16. Bao, X., E. A. Moseman, H. Saito, B. Petryniak, A. Thiriot, S. Hatakeyama, Y. Ito, H. Kawashima, Y. Yamaguchi, J. B. Lowe, et al. 2010. Endothelial heparan sulfate controls chemokine presentation in recruitment of lymphocytes and dendritic cells to lymph nodes. *Immunity* 33: 817–829.
17. Gohda, M., J. Kunisawa, F. Miura, Y. Kagiyama, Y. Kurashima, M. Higuchi, I. Ishikawa, I. Ogahara, and H. Kiyono. 2008. Sphingosine 1-phosphate regulates the egress of IgA plasmablasts from Peyer's patches for intestinal IgA responses. *J. Immunol.* 180: 5335–5343.
18. Kunisawa, J., Y. Kurashima, M. Higuchi, M. Gohda, I. Ishikawa, I. Ogahara, N. Kim, M. Shimizu, and H. Kiyono. 2007. Sphingosine 1-phosphate dependence in the regulation of lymphocyte trafficking to the gut epithelium. *J. Exp. Med.* 204: 2335–2348.
19. Sapoznikov, A., J. A. Fischer, T. Zaft, R. Krauthgamer, A. Dzionek, and S. Jung. 2007. Organ-dependent in vivo priming of naive $CD4^+$, but not $CD8^+$, T cells by plasmacytoid dendritic cells. *J. Exp. Med.* 204: 1923–1933.
20. Kunisawa, J., Y. Kurashima, and H. Kiyono. 2012. Gut-associated lymphoid tissues for the development of oral vaccines. *Adv. Drug Deliv. Rev.* 64: 523–530.
21. Fahlén-Yrlid, L., T. Gustafsson, J. Westlund, A. Holmberg, A. Strömbeck, M. Blomquist, G. G. MacPherson, J. Holmgren, and U. Yrlid. 2009. $CD11c^{high}$ dendritic cells are essential for activation of $CD4^+$ T cells and generation of specific antibodies following mucosal immunization. *J. Immunol.* 183: 5032–5041.
22. Veiga-Fernandes, H., M. C. Coles, K. E. Foster, A. Patel, A. Williams, D. Natarajan, A. Barlow, V. Pachnis, and D. Kioussis. 2007. Tyrosine kinase receptor RET is a key regulator of Peyer's patch organogenesis. *Nature* 446: 547–551.
23. Berndt, B. E., M. Zhang, G. H. Chen, G. B. Huffnagle, and J. Y. Kao. 2007. The role of dendritic cells in the development of acute dextran sulfate sodium colitis. *J. Immunol.* 179: 6255–6262.
24. Luther, S. A., H. L. Tang, P. L. Hyman, A. G. Farr, and J. G. Cyster. 2000. Coexpression of the chemokines ELC and SLC by T zone stromal cells and deletion of the ELC gene in the *plt/plt* mouse. *Proc. Natl. Acad. Sci. USA* 97: 12694–12699.
25. Sallusto, F., B. Palermo, D. Lenig, M. Miettinen, S. Matikainen, I. Julkunen, R. Forster, R. Burgstahler, M. Lipp, and A. Lanzavecchia. 1999. Distinct patterns and kinetics of chemokine production regulate dendritic cell function. *Eur. J. Immunol.* 29: 1617–1625.
26. Proudfoot, A. E., T. M. Handel, Z. Johnson, E. K. Lau, P. LiWang, I. Clark-Lewis, F. Borlat, T. N. Wells, and M. H. Kosco-Vilbois. 2003. Glycosaminoglycan binding and oligomerization are essential for the in vivo activity of certain chemokines. *Proc. Natl. Acad. Sci. USA* 100: 1885–1890.
27. Bromley, S. K., W. R. Burack, K. G. Johnson, K. Somersalo, T. N. Sims, C. Sumen, M. M. Davis, A. S. Shaw, P. M. Allen, and M. L. Dustin. 2001. The immunological synapse. *Annu. Rev. Immunol.* 19: 375–396.
28. Gunn, M. D., V. N. Ngo, K. M. Ansel, E. H. Ekland, J. G. Cyster, and L. T. Williams. 1998. A B-cell-homing chemokine made in lymphoid follicles activates Burkitt's lymphoma receptor-1. *Nature* 391: 799–803.
29. Wendland, M., S. Willenzon, J. Kocks, A. C. Davalos-Misslitz, S. I. Hammerschmidt, K. Schumann, E. Kremmer, M. Sixt, A. Hoffmeyer, O. Pabst, and R. Förster. 2011. Lymph node T cell homeostasis relies on steady state homing of dendritic cells. *Immunity* 35: 945–957.
30. Kolset, S. O., K. Prydz, and G. Pejler. 2004. Intracellular proteoglycans. *Biochem. J.* 379: 217–227.
31. Dagälv, A., K. Holmborn, L. Kjellén, and M. Abrink. 2011. Lowered expression of heparan sulfate/heparin biosynthesis enzyme *N*-deacetylase/*N*-sulfotransferase 1 results in increased sulfation of mast cell heparin. *J. Biol. Chem.* 286: 44433–44440.
32. Lortat-Jacob, H., A. Grosdidier, and A. Imberty. 2002. Structural diversity of heparan sulfate binding domains in chemokines. *Proc. Natl. Acad. Sci. USA* 99: 1229–1234.

OPEN ACCESS Freely available online

PLOS ONE

Potential Roles of CCR5$^+$ CCR6$^+$ Dendritic Cells Induced by Nasal Ovalbumin plus Flt3 Ligand Expressing Adenovirus for Mucosal IgA Responses

Yoshiko Fukuyama[1,2☯], Daisuke Tokuhara[1,2☯], Shinichi Sekine[3], Kazuyoshi Aso[1], Kosuke Kataoka[4], Julia Davydova[5], Masato Yamamoto[5], Rebekah S. Gilbert[1], Yuka Tokuhara[1], Keiko Fujihashi[1], Jun Kunisawa[2,6], Yoshikazu Yuki[2], Hiroshi Kiyono[2], Jerry R. McGhee[1], Kohtaro Fujihashi[1]*

1 Departments of Pediatric Dentistry and Microbiology, The Immunobiology Vaccine Center, The Institute of Oral Health Research, The University of Alabama at Birmingham, Birmingham, Alabama, United States of America, **2** Division of Mucosal Immunology, Institute of Medical Science, University of Tokyo, Tokyo, Japan, **3** Department of Preventive Dentistry, Graduate School of Dentistry, Osaka University, Osaka, Japan, **4** Department of Preventive Dentistry, Institute of Health Biosciences, The University of Tokushima Graduate School, Tokushima, Japan, **5** Department of Surgery, University of Minnesota, Minneapolis, Minnesota, United States of America, **6** Laboratory of Vaccine Materials, National Institute of Biomedical Innovation, Osaka, Japan

Abstract

We assessed the role of CCR5$^+$/CCR6$^+$/CD11b$^+$/CD11c$^+$ dendritic cells (DCs) for induction of ovalbumin (OVA)-specific antibody (Ab) responses following mucosal immunization. Mice given nasal OVA plus an adenovirus expressing Flt3 ligand (Ad-FL) showed early expansion of CCR5$^+$/CCR6$^+$/CD11b$^+$/CD11c$^+$ DCs in nasopharyngeal-associated lymphoid tissue (NALT) and cervical lymph nodes (CLNs). Subsequently, this DC subset became resident in submandibular glands (SMGs) and nasal passages (NPs) in response to high levels of CCR-ligands produced in these tissues. CD11b$^+$/CD11c$^+$ DCs were markedly decreased in both CCR5$^{-/-}$ and CCR6$^{-/-}$ mice. Chimera mice reconstituted with bone marrow cells from CD11c-diphtheria toxin receptor (CD11c-DTR) and CCR5$^{-/-}$ or CD11c-DTR and CCR6$^{-/-}$ mice given nasal OVA plus Ad-FL had elevated plasma IgG, but reduced IgA as well as low anti-OVA secretory IgA (SIgA)Ab responses in saliva and nasal washes. These results suggest that CCR5$^+$CCR6$^+$ DCs play an important role in the induction of Ag-specific SIgA Ab responses.

Citation: Fukuyama Y, Tokuhara D, Sekine S, Aso K, Kataoka K, et al. (2013) Potential Roles of CCR5$^+$ CCR6$^+$ Dendritic Cells Induced by Nasal Ovalbumin plus Flt3 Ligand Expressing Adenovirus for Mucosal IgA Responses. PLoS ONE 8(4): e60453. doi:10.1371/journal.pone.0060453

Editor: Bruno Lourenco Diaz, Universidade Federal do Rio de Janeiro, Brazil

Received December 12, 2012; **Accepted** February 26, 2013; **Published** April 2, 2013

Funding: This work is supported by National Institutes of Health grants DE012242 and AG025873 (http://www.nih.gov/) as well as the Japan Society of the Promotion of Science program entitled "Young Researcher Overseas Visits Program for Vitalizing Brain Circulation"(http://www.jsps.go.jp/english/e-zunoujunkan2/index.html), Global Center of Excellence Program "Center of Education and Research for the Advanced Genome - Based Medicine - For personalized medicine, the control of worldwide infectious diseases - "MEXT" Japan (http://www.jsps.go.jp/english/e-globalcoe/index.html). In addition, a part of studies is supported by the Japan Foundation for Pediatric Research and Houjinkai fellowship award of the Department of Pediatrics at Osaka City University Graduate School of Medicine and The Mochida Memorial Foundation for Medical and Pharmaceutical Research (http://www.mochida.co.jp/zaidan/). The funders had no role in study design, data collection and analysis, decision to publish, or preparation of the manuscript.

Competing Interests: The authors have declared that no competing interests exist.

* E-mail: kohtarof@uab.edu

☯ These authors contributed equally to this work.

Introduction

Nasal delivery of antigen (Ag) given together with a mucosal adjuvant has emerged as an effective way to induce both peripheral and mucosal immunity, including secretory IgA (SIgA) antibody (Ab) responses. In this regard, nasopharyngeal-associated lymphoid tissue (NALT) contains all of the immune cells required for the induction and regulation of the mucosal immune response to Ags delivered into the nasal cavity [1,2]. Our previous studies showed that nasal administration of a naked cDNA plasmid expressing Flt3 ligand cDNA (pFL) enhanced CD4-positive (CD4$^+$) Th2- type cytokine-mediated mucosal immunity and increased lymphoid-type dendritic cell (DC) numbers [3]. Of interest, mucosal delivery of Flt3 ligand cDNA via a recombinant adenovirus (Ad-FL) also exhibited mucosal adjuvanticity through stimulation of NALT DCs [4]. Nasal delivery of ovalbumin (OVA) plus Ad-FL induced CD4$^+$ Th1- and Th2-type responses as well as significant plasma IgG and IgA and SIgA anti-OVA Abs in external secretions. Further, the numbers of CD11b$^+$ CD11c$^+$ DCs expressing high levels of co-stimulatory molecules were preferentially induced. These CD11b$^+$ CD11c$^+$ DCs migrated from the NALT to mucosal effector lymphoid tissues via the cervical lymph nodes (CLNs) [4]. Based upon these findings, we thought it important to determine how chemokines and their receptors affect migration of this DC subset into mucosal effector tissues for the induction of SIgA Ab responses. To pursue this, we assessed chemokine receptors expressed by DCs in both mucosal inductive (NALT) and effector [submandibular glands (SMGs) and nasal passages (NPs)] sites of mice following nasal delivery of OVA and Ad-FL as mucosal adjuvant.

It has been shown that both C-C chemokine receptor (CCR) 6 and CCR7 play important roles in DC relocation and migration both within and between mucosal lymphoid tissues [5,6,7,8,9]. Thus, immature DCs in Peyer's patches (PPs) express CCR6 which controls their movement into the subepithelial dome area [6]. These DCs express CCR7 after Ag uptake, undergo